ARMY RESEARCH LABORATORY

Measured Mass-Normalized Optical Cross Sections For Aerosolized Organophosphorus Chemical Warfare Simulants

by Kristan P. Gurton, Melvin Felton, Rachid Dahmani, and David Ligon

ARL-TR-4220 **August 2007**

NOTICES

Disclaimers

The findings in this report are not to be construed as an official Department of the Army position unless so designated by other authorized documents.

Citation of manufacturer's or trade names does not constitute an official endorsement or approval of the use thereof.

Destroy this report when it is no longer needed. Do not return it to the originator.

Army Research Laboratory
Adelphi, MD 20783-1197

ARL-TR-4220 **August 2007**

Measured Mass-Normalized Optical Cross Sections For Aerosolized Organophosphorus Chemical Warfare Simulants

Kristan P. Gurton, Melvin Felton
Rachid Dahmani, and David Ligon
Computational and Information Sciences Directorate, ARL

REPORT DOCUMENTATION PAGE

Form Approved
OMB No. 0704-0188

1. REPORT DATE *(DD-MM-YYYY)*	2. REPORT TYPE	3. DATES COVERED (From - To)
August 2007	Final	January to October 2006

4. TITLE AND SUBTITLE
Measured Mass-Normalized Optical Cross Sections For Aerosolized Organophosphorus Chemical Warfare Simulants

5a. CONTRACT NUMBER

5b. GRANT NUMBER

5c. PROGRAM ELEMENT NUMBER

6. AUTHOR(S)
Kristan P. Gurton, Melvin Felton, Rachid Dahmani, and David Ligon

5d. PROJECT NUMBER

5e. TASK NUMBER

5f. WORK UNIT NUMBER

7. PERFORMING ORGANIZATION NAME(S) AND ADDRESS(ES)
U.S. Army Research Laboratory
ATTN: AMSRD-ARL-CS-ES
2800 Powder Mill Road
Adelphi, MD 20783-1197

8. PERFORMING ORGANIZATION REPORT NUMBER
ARL-TR-4220

9. SPONSORING/MONITORING AGENCY NAME(S) AND ADDRESS(ES)
U.S. Army Research Laboratory
2800 Powder Mill Road
Adelphi, MD 20783-1197

10. SPONSOR/MONITOR'S ACRONYM(S)

11. SPONSOR/MONITOR'S REPORT NUMBER(S)

12. DISTRIBUTION/AVAILABILITY STATEMENT
Approved for public release; distribution unlimited.

13. SUPPLEMENTARY NOTES

14. ABSTRACT
We present newly measured results of an ongoing experimental program established to measure optical cross sections in the mid and long wave infrared for a variety of chemical and biologically based aerosols. For the present study we consider only chemically derived aerosols, and in particular, a group of chemical compounds often used as simulants for the detection of extremely toxic organophosphorus nerve agents. These materials include; diethyl methylphosphonate (DEMP), dimethyl methylphosphonate (DMMP), diisopropyl methylphosphonate (DIMP), and diethyl phthalate (DEP). As reported in a prior study, we combine two optical techniques well suited for aerosol spectroscopy (i.e., flow-through photoacoustics and FTIR emission spectroscopy), to measure *in situ* the absolute extinction and absorption cross sections over a variety of wavelengths spanning the IR spectral region from 3 to 13 μm. Aerosol size distribution(s), particle number density, and dosimetric measurements are recorded simultaneously in order to present optical cross sections that are aerosol mass normalized, i.e., m^2/gram. Photoacoustic results conducted at a series of CO_2 laser lines, compare well with measured broadband FTIR spectral extinction. Both FTIR and photoacoustic data also compare well with Mie theory calculations based on measured size distributions and previously published complex indices of refraction.

15. SUBJECT TERMS
aerosol, cross-section, extinction, absorption, back-scatter, infrared, DEEP, DIMP, DMMP, DEP

16. Security Classification of:			17. LIMITATION OF ABSTRACT	18. NUMBER OF PAGES	19a. NAME OF RESPONSIBLE PERSON
a. REPORT	b. ABSTRACT	c. THIS PAGE			Kristan P. Gurton
Unclassified	Unclassified	Unclassified	U	40	19b. TELEPHONE NUMBER (*Include area code*) (301) 394-2093

Standard Form 298 (Rev. 8/98)
Prescribed by ANSI Std. Z39.18

Contents

List of Figures **iv**

Acknowledgment **vi**

Introduction **1**

Method **2**

Results **7**

Discussion **12**

References **15**

Appendix A. Complex Indices of Refraction for DIMP, DMMP, DEP (*1*, *2*) **17**

Appendix B. IR Absorptance Spectra for DMMP, DIMP, and DEMP **27**

Distribution List **31**

List of Figures

Figure 1. Schematic of FTIR/photoacoustic experiment used to measure *in situ* the spectral extinction and absorption cross sections. 3

Figure 2. Cross sectional schematic of a top set of acoustic dampeners used to isolate the electret inner cavity. 4

Figure 3. Typical size distribution for the aerosolized chemical simulant. 7

Figure 4. Measured FTIR (solid line) and photoacoustic (data points) derived mass-normalized extinction and absorption cross sections for DMMP. Also shown are the corresponding Mie theory calculations for the spectral extinction and absorption (dashed lines) based on the size distribution shown in figure 3 and previously published indices of refraction (*11*). 9

Figure 5. Measured mass-normalized FTIR spectral extinction (solid line) from 3 to 13 μm for DMMP. Also shown are the corresponding Mie theory calculations (dashed lines) for the spectral extinction, absorption, total scatter, and backscatter based on the size distribution shown in figure 3 and previously published indices of refraction (*11*). 9

Figure 6. Measured FTIR (solid line) and photoacoustic (data points) derived mass-normalized extinction and absorption cross sections for DIMP. Also shown are the corresponding Mie theory calculations for the spectral extinction and absorption (dashed line) based on the size distribution shown in figure 3 and previously published indices of refraction (*11*). 10

Figure 7. Measured mass-normalized FTIR spectral extinction (solid line) from 3 to 13 μm for DIMP. Also shown are the corresponding Mie theory calculations (dashed lines) for the spectral extinction, absorption, total scatter, and backscatter based on the size distribution shown in figure 3 and previously published indices of refraction (*11*). 10

Figure 8. Measured FTIR (solid line) and photoacoustic (data points) derived mass normalized extinction and absorption cross sections for DEP. Also shown are the corresponding Mie theory calculations for the spectral extinction and absorption (dashed lines) based on the size distribution shown in figure 3 and previously published indices of refraction (*11*). 11

Figure 9. Measured mass-normalized FTIR spectral extinction (solid line) from 3 to 13 μm for DEP. Also shown are the corresponding Mie theory calculations (dashed lines) for the spectral extinction, absorption, total scatter, and backscatter based on the size distribution shown in figure 3 and previously published indices of refraction (*11*). 11

Figure 10. Measured FTIR (solid line) and photoacoustic (data points) derived mass-normalized extinction and absorption cross sections for DEMP. Representative size distribution 5 for the FTIR measurement can be seen in figure 2. Because no complex indices of refraction were available, no corresponding Mie theory calculations were conducted for DEMP. 12

Figure 11. Various phase states for chemical agents during dispersion. 13

Figure B-1. Measured absorptance spectra for 1 cm path of liquid phase dimethyl-methylphosphonate (DMMP). 27

Figure B-2. Measured absorptance spectra for 1 cm path of liquid phase diisopropyl-methylphosphonate (DIMP).....28
Figure B-3. Measured absorptance spectra for 1 cm path of liquid diethyl methylphosphonate (DEMP). 29

Acknowledgment

We would like to thank both the Air Force Research Laboratory (AFRL) and the Edgewood Chemical and Biological Command (ECBC) for their continued support and technical expertise.

Introduction

Currently there is great interest in developing new methods to safely detect the presences of airborne toxins. Light Detection and Ranging (LIDAR) systems have long been used to detect and map the presence of man-made and naturally occurring gas and aerosol concentrations in the open atmosphere (*1*, *2*, *3*). Recently Fourier transform infrared spectroscopy (FTIR) studies have identified unique spectral absorption/emission and backscatter characteristics for a variety of chemical and biological aerosols in the mid and long-wave IR (*4*, *5*). However, the ability for such systems to take advantage of this spectral information will require multiple (or broadly tunable) laser sources that span a significant portion of the mid to long wave IR region of the spectrum. Current LIDAR systems designed for aerosol applications are usually limited to either near IR wavelengths (typically between 1 and 2 μm), or take advantage of the limited tunability between 9.2 and 10.8 μm associated with conventional CO_2 lasers (*3*). However, with the advent of a relatively new class of solid state Quantum Cascade Lasers (QCL), coherent sources, with reasonable power and available for practically any wavelength between 3 and 17 μm, are becoming readily available (*6*, *7*).

As a result, new Chemical and Biological Warfare (CBW) agent "standoff" and "point" detection approaches and instrumentation are being considered, e.g., multi-wavelength or frequency agile LIDAR systems (*8*). In order to design and implement the various optically based detection methods being proposed, a reliable database of optical parameters is needed that encompass a variety of CBW related aerosols. Unfortunately, such information is lacking and is particularly sparce for biologically derived aerosols.

In order to address this need, we have conducted a set of complimentary measurements that include conventional FTIR aerosol spectroscopy and flow-through photoacoustics designed to provide well calibrated optical cross sections in the IR wavelength region, 3 to 13 μm. This report represents a continuation of prior work in which mass normalized cross sections were measured and calculated for a variety of biological and inorganic particulates (*9*, *10*). Although the experimental techniques used here are described in detail in prior reports, for completeness, we will briefly outline the methods and procedures used for both the broadband FTIR-based measurement and the single wavelength photoacoustic technique.

In order to simultaneously measure the absolute extinction and absorption (and subsequently the total scatter via the difference) we employ two independent optical techniques which probe the same dispersed *in situ* aerosol volume, i.e., FTIR and flow-through photoacoustic aerosol spectroscopy. For the present study, we measure a path-integrated spectral extinction, $\varepsilon(\lambda)$, from 3 to 13 μm using an FTIR spectrometer that is operating in an emission mode, while the total absorption and extinction is measured using the photoacoustic technique at various single CO_2

laser-line wavelengths between 9.2 and 10.8 μm, i.e., α(λ1), α(λ2), α(λ3), …. ε(λ1), ε(λ2), ε(λ3), etc.

For chemical simulants in which the complex indices of refraction are available (*11*), Mie theory calculations are carried out over the same wavelength range by applying the indices with the measured aerosol size distribution. Finally, calculated total extinction, absorption, scatter, and backscatter cross sections are compared with values obtained from the FTIR/Photoacoustic portion of the experiment.

Rather than working with the extremely toxic organophosphate derived "nerve" agents themselves, such as Soman (GD), or Sarin (GB), it is desirable to identify and work with more mundane "simulant" chemical compounds that exhibit similar molecular features. As a result a series of simulant materials have been identified that exhibit the same vibrational/rotational molecular behavior seen in the actual true toxins that are typically associated with Phosphorous Oxygen Carbon (POC) group(s).

We chose four of the most commonly accepted nerve agent simulants for examination, i.e., dimethyl methylphosphonate (DMMP), diethyl methylphosphonate (DEMP), diisopropyl methylphosphonate (DIMP), and diethyl phthalate (DEP). These simulants posses the same P-O and P-C bonds seen in Sarin, Soman or V-series (VX) agents, yet lack the extremely reactive P-F bonds seen in actual nerve agents and are therefore considered much safer for laboratory analysis.

Method

Because the basic approach used for this study has been well documented elsewhere (*4*, *5*, *9*, *12*), only a general description of the experimental and analytical techniques will be outlined here. The basic FTIR/photoacoustic aerosol measurement is shown in figure 1.

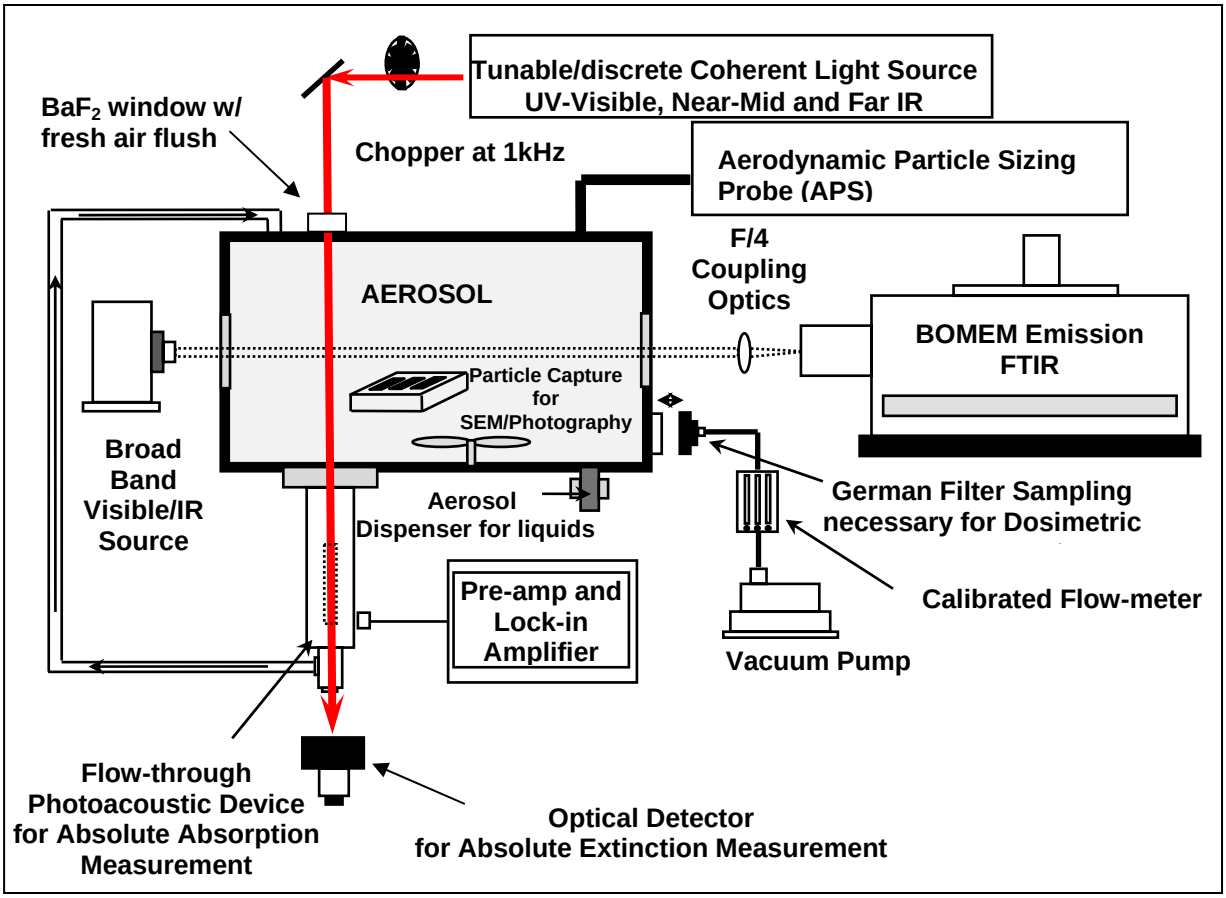

Figure 1. Schematic of FTIR/photoacoustic experiment used to measure *in situ* the spectral extinction and absorption cross sections.

As seen in figure 1, the system consists of a small aerosol chamber (approx. 0.4 m^3) where the chemical simulant is nebulized and uniformly dispersed using a low-velocity fan. A cylindrical flow-through photoacoustic "spectrophone" is mounted to the bottom of the chamber. Once dispersed, the aerosol is gently drawn down through a hollow region that runs axially through the device. A modulated CW CO_2 laser, tuned to a specific IR wavelength, is directed through a BaF_2 window located at the top of the chamber. The beam is directed down into the chamber and through the center of the spectrophone which contains the particle-air mixture. The beam exits through a windowless region located at the bottom of the spectrophone and attenuation of the laser power due to extinction by the aerosol is measured by a caloric IR detector located near the beam exit. Laser power is kept relatively low (typically less than 200 mW) to avoid phase changes associated with particle vaporization. At the center of the spectrophone cylinder is a small electret microphone that is embedded into the wall of the inner cavity.

Ambient acoustic noise resulting from activity within the laboratory is suppressed by a series of acoustic dampeners located above and below the electret microphone (see figure 2). Figure 2

shows a cross sectional view of a top set of three cylindrical acoustic dampeners. These dampeners fit snuggly together in the region surrounding the inner electret cavity and serve to dissipate the acoustic noise which enters the spectrophone from either opening. Acoustic noise due to activities within the laboratory flow freely through the center cylindrical region of the spectrophone. Acoustic noise enters the spectrophone in the form of pressure fluctuations that are initially distributed over the area of the inlet nozzle shown as point A, in figure 2. For our example, define the area at point A to be 1.0 cm^2. As the pressure-wave propagates down toward the inner electret cavity, it encounters several enlarged openings at point(s) B, in the figure. At these points the pressure wave is effectively redistributed over a much larger area, approximately 5.0 cm^2, resulting in a reduction of the net pressure. The attenuation of the noise signal is repeated at each slit B until the desired noise suppression is achieved.

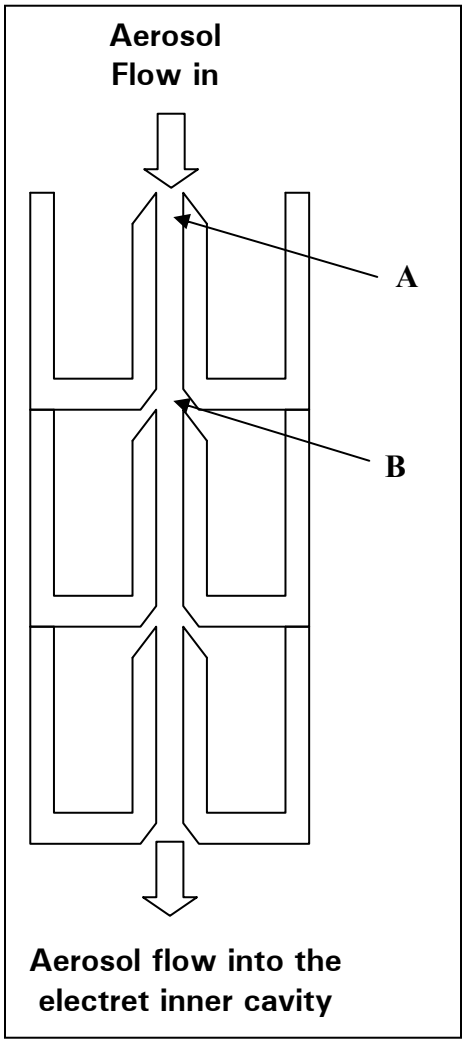

Figure 2. Cross sectional schematic of a top set of acoustic dampeners used to isolate the electret inner cavity.

We have found that a series of three or four dampeners placed above and below the electret cavity are sufficient to suppress typical noises levels encountered in the laboratory by approximately 20 dB at 1 kHz. Additionally, isolation is accomplished by machining the spectrophone enclosure from very dense materials, e.g., stainless steel or high density polyurethane.

The basic principle behind aerosol photoacoustics is best explained by considering a simple example. Let us assume a sample volume containing an polydisperse distribution of optically absorbing aerosol particles. If a modulated laser is passed through this volume, the energy will be attenuated by a combination of particle scattering and absorption. The absorption results in a rapid heating and subsequent cooling of the particle-air mixture as the laser beam undergoes several duty cycles of the modulated laser (here we assume that the molecular absorption due to the surrounding gas is negligible compared to the resultant absorption by the particles). This cyclic heating/cooling of the aerosol mixture results in a pressure wave in the immediate region where the laser and aerosol interact. If the laser is modulated at some convenient acoustic frequency, 1 kHz for example, a resultant pressure wave will produce an acoustic signal at the same 1 kHz modulation frequency. The resultant acoustic signal can then be detected by the electret microphone. The electret produces an electrical signal, which is proportional to the absorbed energy and is amplified many orders of magnitude via a lock-in amplifier that is tuned to the 1 kHz frequency (*13*, *14*).

The responsivity and calibration of the photoacoustic device is achieved by designing the system such that the probe laser (in this case a tunable CO_2 laser) also serves as a coincident short-pass transmissometer. Here the attenuating path of the transmissometer is defined from the top of the aerosol chamber, where the beam enters, and ends at a well defined point near the exit port where the aerosol is drawn from the system. By applying a simple Beer's law relation, the arrangement allows for an independent measurement of the absolute path-integrated extinction coefficient, $\varepsilon(1/m)$, that is used to calibrate the photoacoustic device.

Calibration is carried out by substituting the aerosol with an absorbing gas. The calibration gas is drawn through the flow-through photoacoustic device in the exact same manner as the aerosol. However, now all of the extinction measured by the transmissometer results from absorption only of the calibration gas since there is no particulate scattering present (here we have assumed that molecular scattering is negligible when compared with the optical absorption). As with the aerosol, a rapid heating and cooling cycle occurs within the region near the electret. Again, an acoustic signal results and is detected and amplified, and is taken to be proportional to the optical absorption of the gas.

Because there is no scattering during the calibration process, the total measured extinction (via the short-path transmissometer) is due solely to the absorption by the calibration gas. By equating the path-integrated extinction to the total absorption, we have $\varepsilon(1/m) = \alpha(1/m)$, where

α(1/m) in now taken to be the path-integrated absorption. For each particular extinction coefficient, a corresponding acoustic signal is detected and recorded. The calibration process is repeated for different concentrations of gas and a plot of the spectrophone signal versus path-integrated absorption (or extinction) is generated. The slope of this response curve represents a calibration constant relating aerosol absorption to spectrophone signal. Although any appropriately absorbing gas may be used to calibrate the device, we have found for operation in the LWIR that isopropanol alcohol vapor works well as an efficient absorbing gas for all CO_2 laser wavelengths considered.

The broadband IR spectral extinction is measured using a high-resolution (0.02 wave-number) Bomem MR Series FTIR spectrometer. A radiometrically stabilized IR Nernst glow-bar is used as the broadband source. The broadband energy is collimated and projected through the aerosol chamber via two BaF_2 transmission windows. All transmission windows are fitted with dry-air flushes to eliminate contamination due to aerosol build up. The broadband IR source is coupled to the FTIR spectrometer using a gold-surfaced, f/4, off-axis parabola. Because aerosol spectra are usually devoid of any sharp features (compared to spectra derived from gases), the spectrometer is operated at a moderate spectral resolution of 8 cm^{-1}.

The liquid chemical simulants are aerosolized within the chamber using a DeVilbiss pharmaceutical nebulizer. Approximately 20 psi of dry air is used to pump the nebulizer during dispersion. This results in a highly reproducible size distribution with particles predominately in the 6-μm range or less. Aerodynamic particle size distributions are measured continuously using an Aerodynamic Particle Sizer (APS), Model 3321, manufactured by TSI Inc. Particle aerodynamic derived diameters are converted to geometric diameters using the relation, $d(aero) = d(geo)\sqrt{\rho/\mathrm{X}}$, where ρ is the bulk density of the simulant and X is an aerodynamic form factor which is taken to be 1 for perfect spheres. A typical size distribution resulting from the nebulizer is shown in figure 3. Note that once the aerosol chamber had reached equilibrium, i.e., number of particles being generated by the nebulizer equals number of particles being lost due to impacting with the chamber walls and/or fan, the size distributions remained exceptionally stable during the entire run. Similarly, because each of the four chemicals had very nearly identical viscosities and vapor pressures, and because great care was taken to ensure nebulizer pressure remained constant between measurements, the distribution seen in the figure 3 is a reasonable representation for all simulants considered and for all measurements conducted.

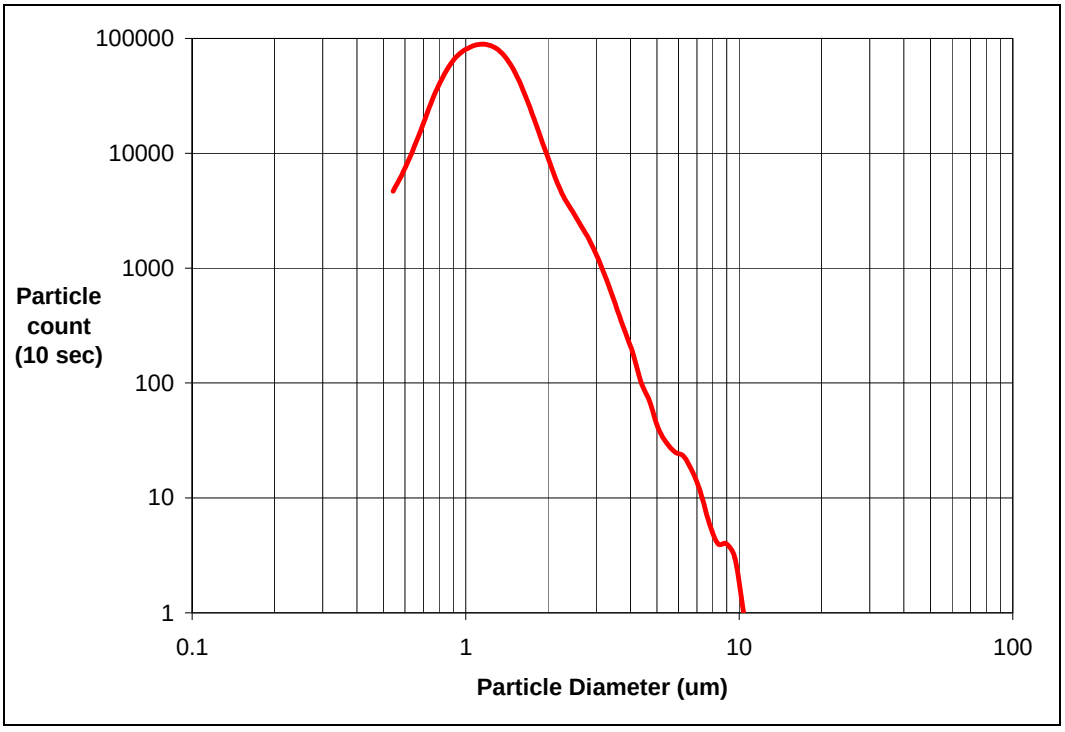

Figure 3. Typical size distribution for the aerosolized chemical simulant.

Aerosol mass densities (g/m^3) are periodically measured during each run using conventional dosimetric techniques. Aerosol mass samples are continuously collected during the photoacoustic/FTIR measurements by drawing known volumes of the air-particle mixture onto polycarbonate filters (nominal pore-size 0.20 μm), for predetermined periods of time. Mass samples are then weighed and used to convert path-integrated extinction and absorption cross sections (1/m), into the more useful mass normalized quantities (m^2/g).

Results

The four nerve agent simulants considered for this study include dimethyl methylphosphonate (DMMP) CAS#756-79-6 (simulant for Sarin), diethyl phosphonate (DEMP) CAS#683-08-9 (simulant for Sarin), both purchased from Fluka Inc., diisopropyl phosphonate (DIMP) CAS#1445-75-6 (simulant for Soman), which was purchased from Lancaster Synthesis, Inc., and diethyl phthalate (DEP) CAS#84-66-2 (simulant for V-series VX nerve agents), purchased from Sigma-Aldrich, Inc. All four liquid chemicals possess no noticeable color or odor and all exhibit relatively low vapor pressure.

In order to avoid confusion, the spectra from each simulant is displayed in two graphs. The first graph displays the laser-line measurements of the photoacoustic study from 9 to 11 μm, and the corresponding broad band spectral extinction obtained from the FTIR and corresponding Mie theory calculations. The second graph displays an expanded view (range from 3 to 13 μm) of the broad band spectral extinction, absorption, total scatter, and the differential backscatter, obtained from the FTIR work and Mie theory calculations. Unfortunately, Mie theory calculations could not be conducted for DEMP shown in figure 10 because complex indices of refraction for this material were not available. For all transmission type measurements, i.e., both FTIR and CO_2 laser line extinction, a forward scatter correction is applied (*15*). In all cases this correction is relatively small beyond 7 to 8 μm. Note that for all simulants considered here, the complex portion of the index of refraction, which is directly related to the optical absorption, was extremely small-in the approximate region 3.5 to 6.5 μm. As a result, the spurious behavior of Mie calculated absorption for this region, as seen in figures 5, 7, 9, is effectively taken to be zero. As shown in figures 4 through 10, results of the FTIR and photoacoustic measurements agree reasonably well with the Mie calculated values with the exception the DEP spectra shown in figure 8. Here one can see a divergence between measured and Mie calculated absorption between 10 and 11 μm. Although the overall trend downwards appear similar, the magnitudes of the values differ greatly. After thorough review we believe the discrepancy arises from the fact that the absorption values beyond 10 μm are relatively small. As a result, large uncertainties exist for both the measured photoacoustic results and in the methods used by Querry to determine the complex indices of refraction used in the Mie calculations (*11*). At such low levels of absorption, small uncertainties in the values of the complex portion of the index result in large variation in the Mie calculated values of the absorption. After review we attribute the disagreement between measured and calculated absorption for the last two data points seen in figure 8, to a low signal-to-noise region inherent in both studies and thus not entirely unexpected. For completeness we have included in appendix A the tabular values of the complex refractive indices taken from Querry (*11*).

DMMP

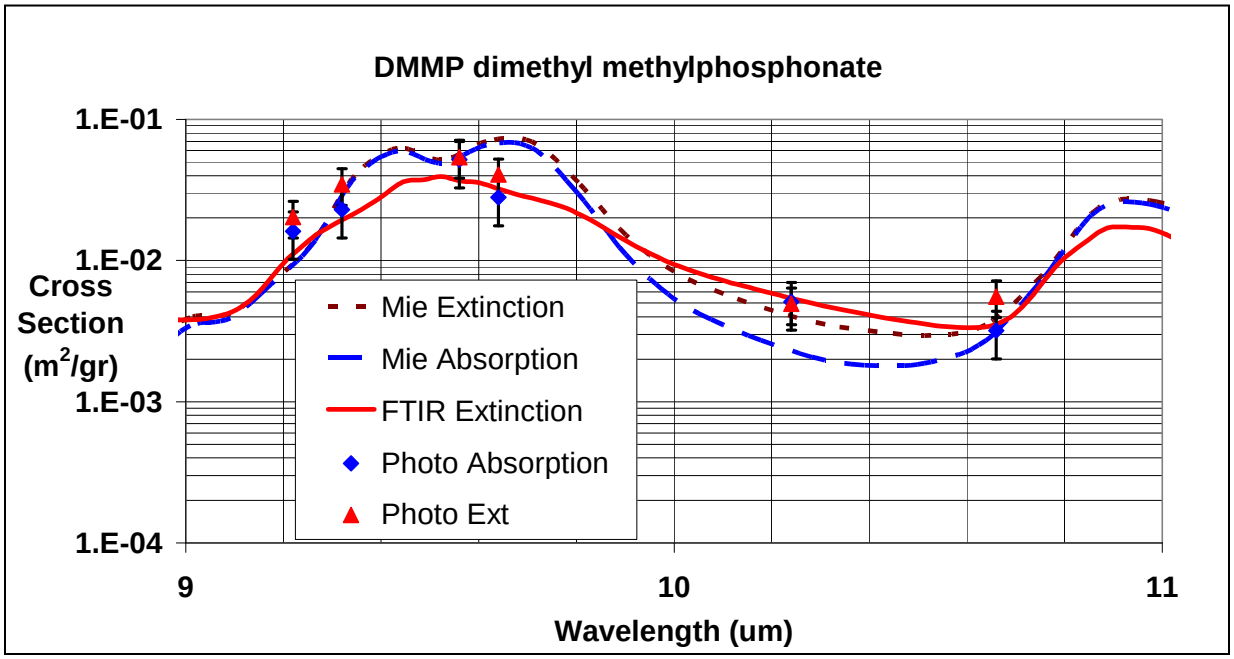

Figure 4. Measured FTIR (solid line) and photoacoustic (data points) derived mass-normalized extinction and absorption cross sections for DMMP. Also shown are the corresponding Mie theory calculations for the spectral extinction and absorption (dashed lines) based on the size distribution shown in figure 3 and previously published indices of refraction (*11*).

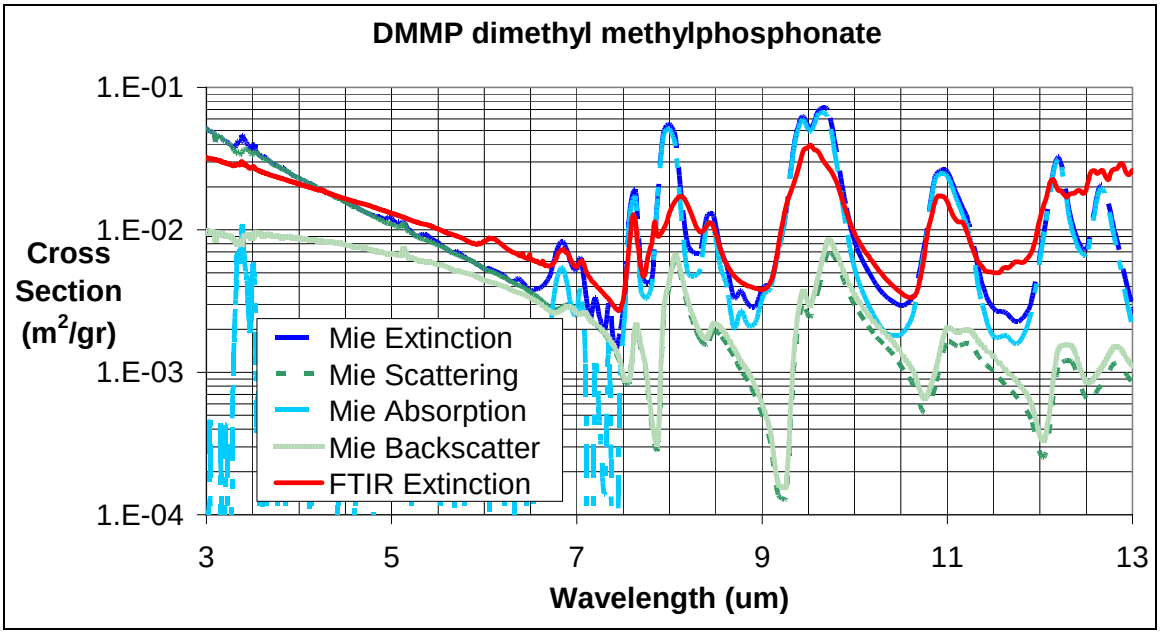

Figure 5. Measured mass-normalized FTIR spectral extinction (solid line) from 3 to 13 μm for DMMP. Also shown are the corresponding Mie theory calculations (dashed lines) for the spectral extinction, absorption, total scatter, and backscatter based on the size distribution shown in figure 3 and previously published indices of refraction (*11*).

DIMP

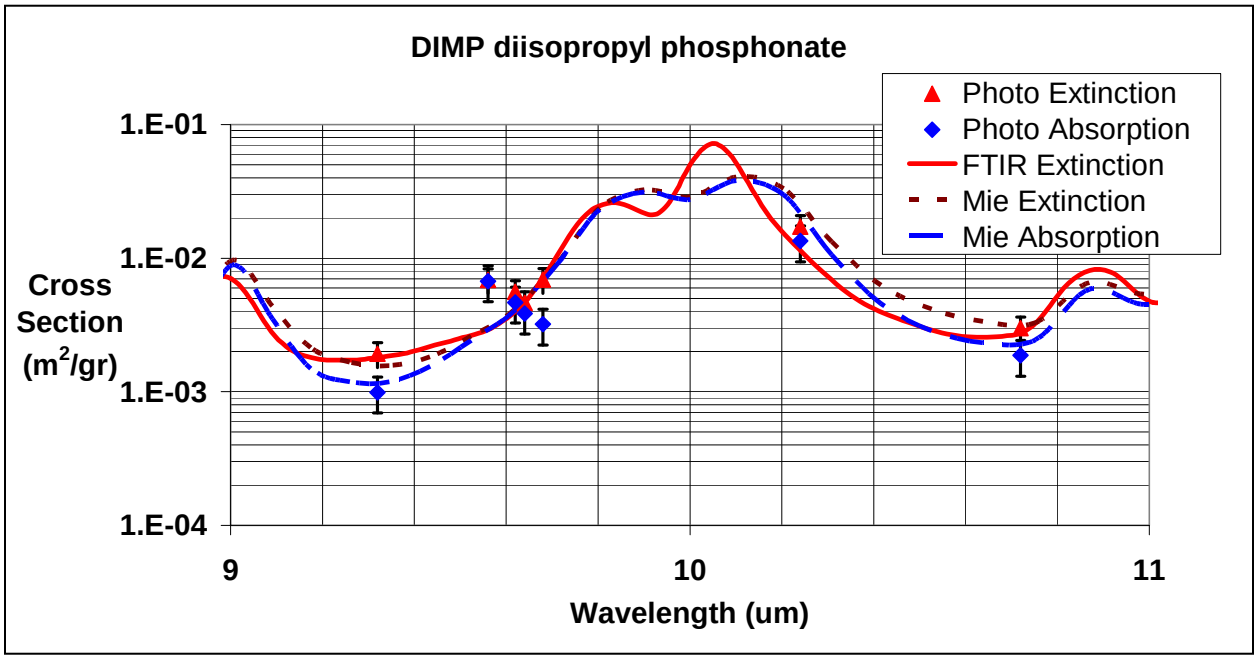

Figure 6. Measured FTIR (solid line) and photoacoustic (data points) derived mass-normalized extinction and absorption cross sections for DIMP. Also shown are the corresponding Mie theory calculations for the spectral extinction and absorption (dashed line) based on the size distribution shown in figure 3 and previously published indices of refraction (*11*).

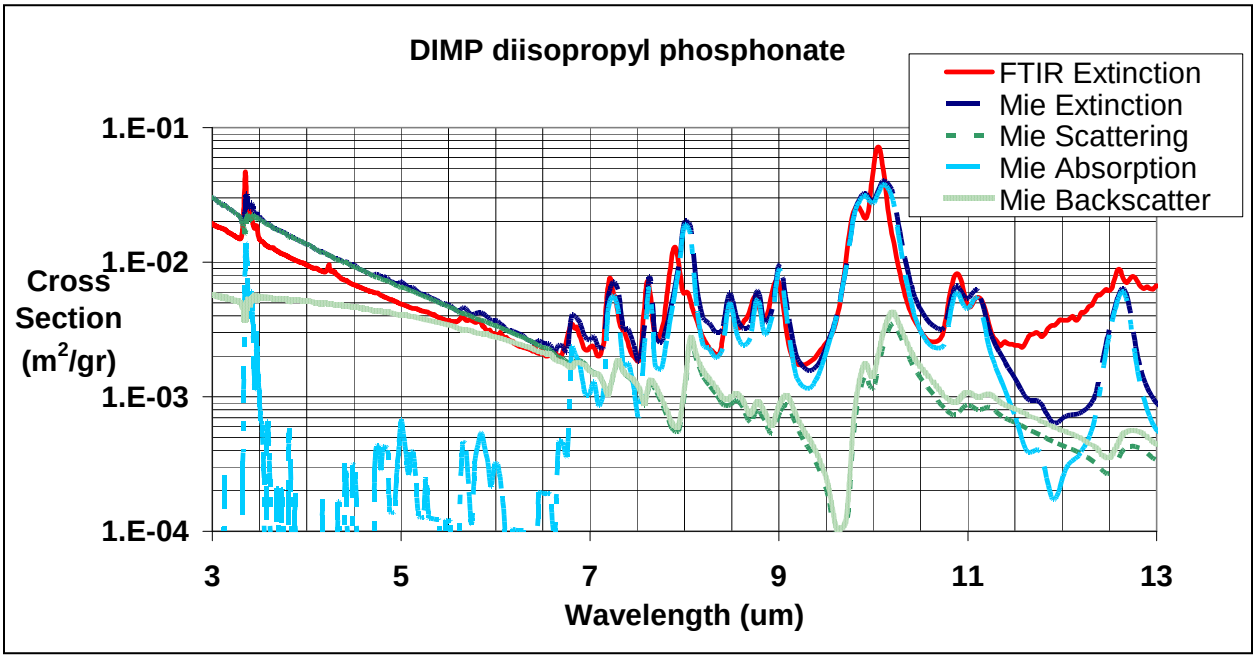

Figure 7. Measured mass-normalized FTIR spectral extinction (solid line) from 3 to 13 μm for DIMP. Also shown are the corresponding Mie theory calculations (dashed lines) for the spectral extinction, absorption, total scatter, and backscatter based on the size distribution shown in figure 3 and previously published indices of refraction (*11*).

DEP

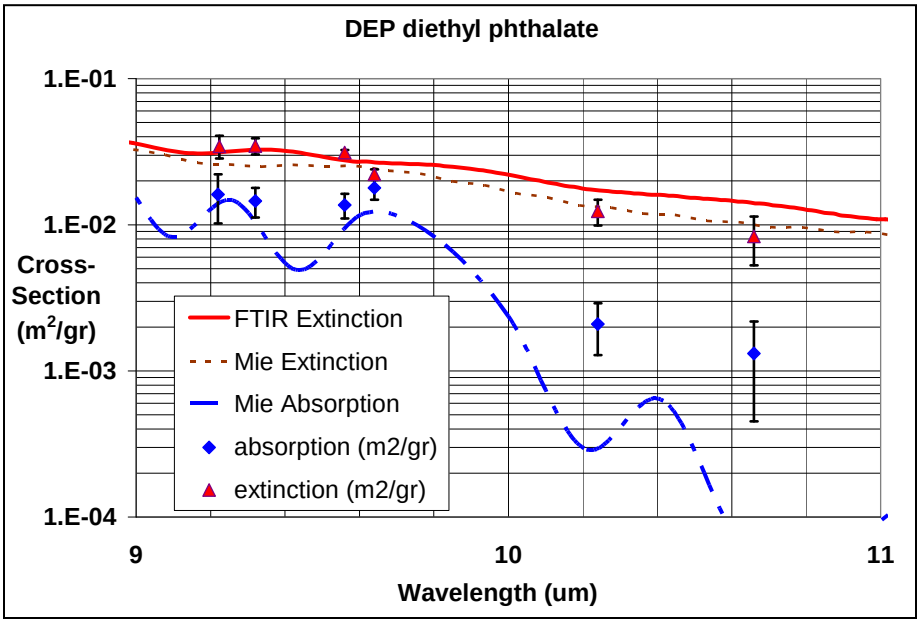

Figure 8. Measured FTIR (solid line) and photoacoustic (data points) derived mass normalized extinction and absorption cross sections for DEP. Also shown are the corresponding Mie theory calculations for the spectral extinction and absorption (dashed lines) based on the size distribution shown in figure 3 and previously published indices of refraction (*11*).

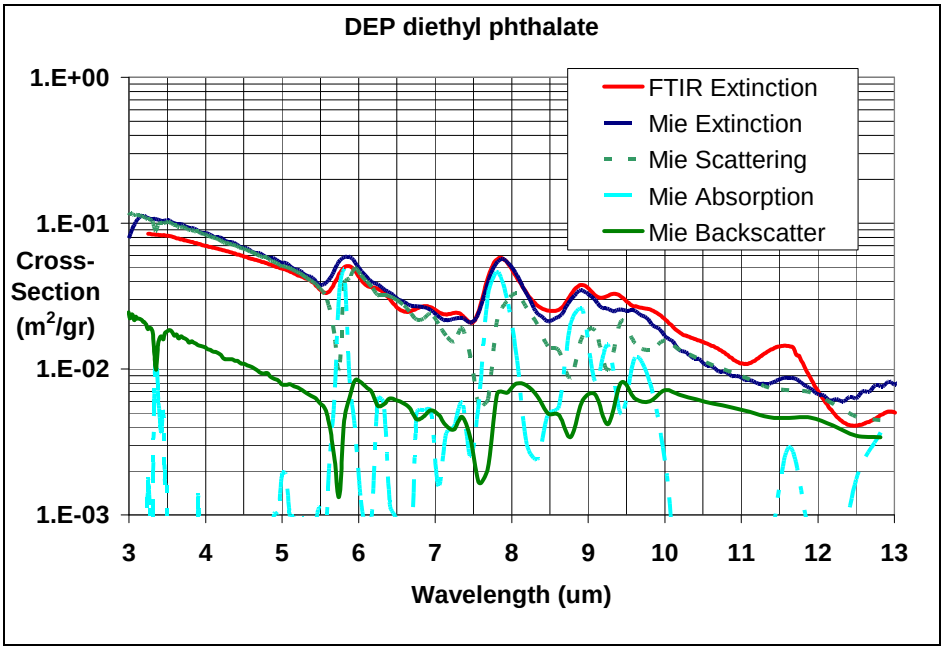

Figure 9. Measured mass-normalized FTIR spectral extinction (solid line) from 3 to 13 μm for DEP. Also shown are the corresponding Mie theory calculations (dashed lines) for the spectral extinction, absorption, total scatter, and backscatter based on the size distribution shown in figure 3 and previously published indices of refraction (*11*).

DEMP

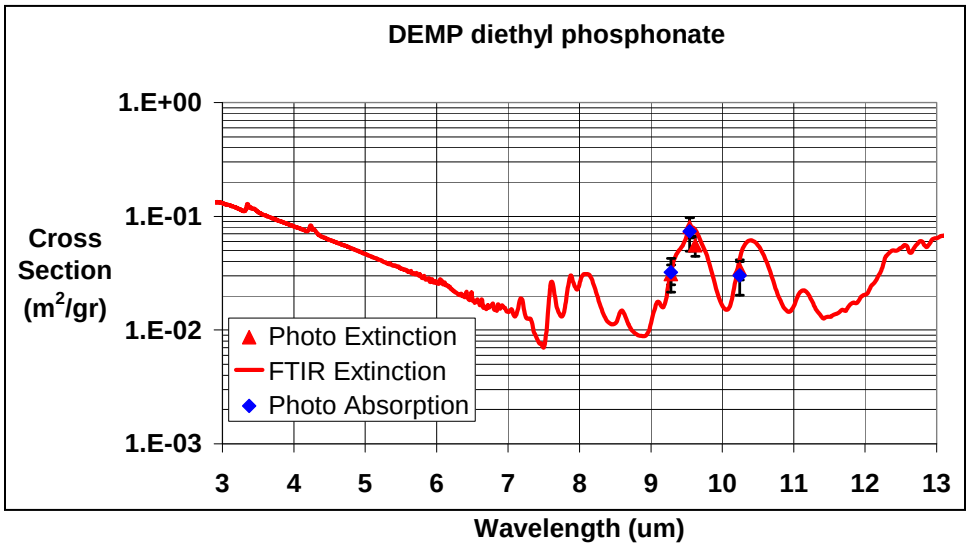

Figure 10. Measured FTIR (solid line) and photoacoustic (data points) derived mass-normalized extinction and absorption cross sections for DEMP. Representative size distribution 5 for the FTIR measurement can be seen in figure 2. Because no complex indices of refraction were available, no corresponding Mie theory calculations were conducted for DEMP.

Discussion

At this point it is useful to discuss the effect of phase state of the chemical agent and/or particle size distributions on various optical properties in the IR. So far we have focused on four specific chemical agents, and in particular, in aerosol form. However, from the standpoint of detection of a particular agent, the phase of the material is just as important of a factor as chemical composition. Depending on how the agent is dispersed, the phase state of chemical may include vapor, liquid, thickened liquid (which may produce vapor also), small and large sized aerosol particles, and rain-sized droplets. A schematic showing a possible scenario in which all phase states are present is shown in figure 11.

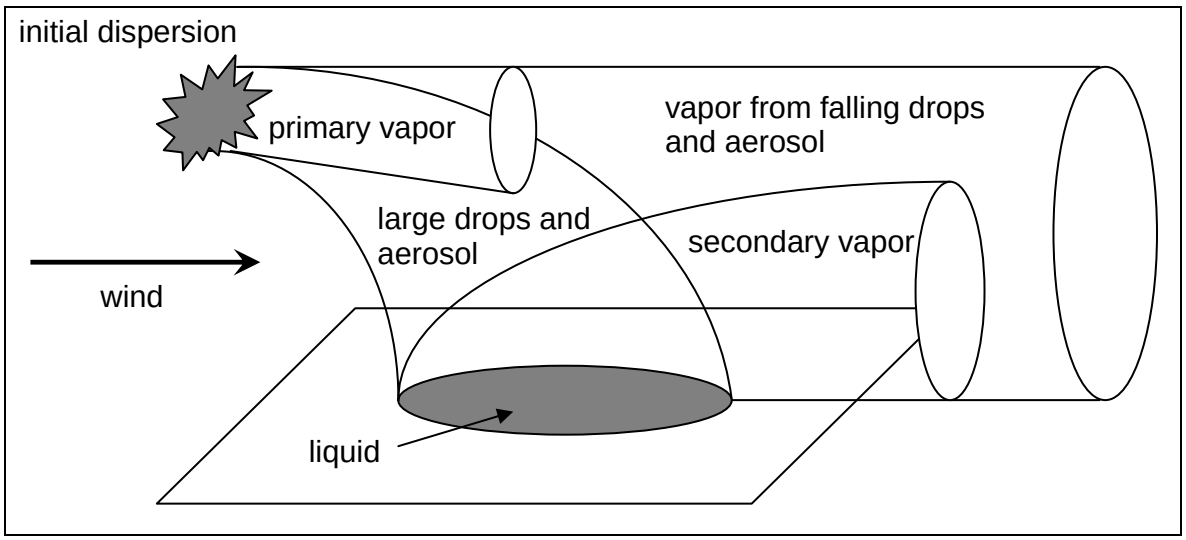

Figure 11. Various phase states for chemical agents during dispersion.

Flanigan has reported only minor differences between liquid and vapor phase for measured IR absorption spectra for a variety of chemical agents (*16*, *17*). At first glance one might find this peculiar, since it is well known that IR spectra of diatomic and simple polyatomic vapor molecules generally exhibit significantly more fine line structure when compared to spectra derived from liquids. However, for complex molecular compounds like the simulants considered here, the spacing between lines become reduced, and for asymmetric molecules the position of these lines become quite random. The net effect is that the spectral lines appear to overlay one another and are rarely able to be resolved with conventional spectroscopy. It is for this reason that the vapor/gaseous spectrum for most chemical agents (which tend to be highly asymmetric) lack the fine line structure often observed in other gaseous media.

For aerosols and/or droplets, scattering becomes an important component to the total extinction and factors such as particle size and shape become important. This is particularly true as the predominate particle size become comparable to the wavelength. As a result, a small variation in the particle side distribution can have dramatic effects on the various spectral components. Therefore, when designing aerosol detection systems which relies on cues from a particular absorption, extinction, or backscatter feature, reasonable accuracy of the expected sized distribution is usually required.

It should be obvious that, based on the previous few paragraphs, one should be careful when designing systems to exploit a particular spectral feature, to ensure the measured phase state matches that of the anticipate application. For example, one might consider absorption spectra derived from vapor or liquid, if the application is to detect CBW surface contamination. However, the use of the same spectra for developing an aerosol detection scheme would not be appropriate. Unfortunately, this mistake is more common than one might expect. Errors resulting from phase state mismatch is most common for application dealing with obscure materials in which good extinction or absorption spectra (for a particular phase) does not exist

and spectra derived from a different state is knowingly (or unknowingly) applied. This is particularly true for biological materials where the existing measured IR spectra is still quite sparse (*18*, *19*, *20*).

For completeness and comparison with measured aerosol spectra seen in figures 4 through 10, we show the absorptance spectra measured for liquid DEMP, DMMP, and DIMP simulants (see appendix B (*11*, *21*)). Unfortunately, due to a technical problem that arose with the FTIR spectrometer, we were unable to measure the absorptance spectra for the chemical simulant DEP and thus it is not shown.

Finally, a few general comments on how the various spectral features seen in figures 4 through 10 are effected by differing size distributions. In order to proceed, let us define three different distributions based on the nominal size of the particles, when compared to mid or long wave IR wavelengths. For such a wavelength region we define three aerosols distributions as small (nominal particle dia. < 2 μm), intermediate (nominal particle dia. between 2 to 30 μm), and large or droplet size (particle dia. > 30 μm). For the current study we intentionally generated particles with sizes that lie within the "intermediate" range since it is considered the most probable scenario that one might expect in practice.

If the expected particle sizes tend towards a "small" distribution, the contribution due to scattering will be greatly reduced and spectral features for both extinction and absorption (or emission for the IR) will dominate. As a result, the differences between peaks and valleys of the spectra, seen in figures 4 through 10 for those components, will increase and look very similar to the type of spectrum derived for a vapor phase.

For size distributions that tend towards the "large" size (but still not characterized as droplets, e.g., 10 to 30 μm range), particle scattering increases rapidly and the spectral features seen in figures 4 through 10 will become less prominent for the extinction and absorption with the absorption (and emission) retaining spectral features a bit longer than that of the extinction. Also, as the particle sizes increase, the expected backscatter spectra will shift slowly towards the longer wavelengths.

For particles that are best characterized as "droplets" (30 to 100 μm) detection schemes based on the identification of certain spectral features are considered to be useless since the resultant spectra for these sized particles are nearly flat. However, there still exists reasonable backscatter structure that remains relatively constant although slightly shifted towards longer wavelengths. As result, a multi-spectral IR LIDAR detection approach seems reasonable since the expected backscatter response would be relatively predictable over a wide range of particle sizes. This approach could be strengthened/complimented by including a "passive" muti-spectral IR imaging approach since absorption/emission spectral features hold up fairly well (particularly in the LWIR region) over a similar range of particle size distributions.

References

1. Ben-David, A. Backscatter measurements of the atmospheric aerosols at CO2 laser wavelengths: implications of aerosol spectral structure on differential-absorption LIDAR retrievals of molecular species. *Appl. Opt.* **1999**, *38* (12), 2616–2624.

2. Koch, Grady J.; Barnes, Bruce W.; Petros, Mulugeta; Beyon, Jeffrey Y. Coherent Differential Absorption Lidar Measurements of CO2. *Appl. Opt.* **2004,** *43* (26), 5092–5099.

3. Vanderbeek, R.; Gurton, K. Backscatter Measurements of Aerosolized CB Simulants with a Frequency Agile CO2 Lidar. *SPIE International Symposium Photonics East,* Providence, Rhode Island USA, October 27–30, 2003.

4. Gurton, K. P.; Dahmani, R.; Ligon, D. Measured IR optical cross sections for a variety of chemical and biological aerosol simulants. *Appl. Opt.* **2004**, *43* (23), 4564–4570.

5. Gurton, Kristan P.; Ligon, David; Kvavilashvili, Ramaz. Measured Infrared Spectral Extinction for Aerosolized Bacillus subtilis var. niger endospores from 3 to 13 μm. *Applied Optics* **2001**, *40* (25), 4443–4448.

6. Faist, J.; Capasso, F.; Sortpro, C.; Baillargeon, J.; Hutchinson, A. L.; Chu, S.; Cho, A. Quantum design of QC-laser. *Appl. Phys. Lett.* **1960**, *68*, 3680–3682.

7. Totchnig, G.; Winter, F.; Pustogov, V.; Faist, J.; Miller, A. Mid-infrared external-cavity quantum-cascade laser. *Opt. Letters* **2002**, *27* (20), 1788–1794.

8. Carrico, J. P. The DOD chemical-biological stand-off detection program: a revisit nearly ten year later. Third Workshop on Stand-off Detection for Chemical and Biological Defense, Williamsburg, VA, 17–21 October 1994

9. Gurton, K. P.; Dahmani, R.; Ligon, D.; Bronk, B. In situ measurement of the optical absorption and extinction for chemical and biologically derived aerosols using flow-through photoacoustics. *Appl. Opt.* **2005**, *44* (19), 4001–4006.

10. Gurton, Kristan P.; Ligon, David; Dahmani, Rachid *In situ measurement of the infrared spectral extinction for various chemical, biological, and background aerosols*; ARL-TR-3071; U.S. Army Research Laboratory: Adelphi, MD, September 2003.

11. Querry, Marvin R. *Optical constants of minerals and other materials from the millimeter to the ultraviolet*; Chemical Research, Development and Engineering Center technical report, CRDEC-CR88009, November 1987.

12. Gurton, K. P.; Dahmani, R.; Ligon, D.; Bronk, B. *Measured IR absorption and extinction cross sections for a variety of chemically and biologically derived aerosol simulants*; ARL-TR-3253; U.S. Army Research Laboratory: Adelphi, MD, June 2004.

13. Pao, Y. *Optoacoustic Spectroscopy and Detection*; Academic Press, New York, 1977.

14. Rosencwaig, A. *Photoacoustics and Photoacoustic Spectroscopy*; John Wiley & Sons, New York, 1980.

15. Deepak, A.; Box, M. Forwardscattering correction for optical extinction measurements in aerosol media. 2: Polydispersion. *Appl. Opt.* **1978**, *17* (19), 3169–3176.

16. Flanigan, D. F. *The Spectral Signatures of Chemical Agent Vapors and Aerosols*; U.S. Army Chemical Research and Development Center Technical Report # CRDC-TR-85002: April 1985.

17. Flanigan, D. F. Hazardous cloud imaging: a new way of using passive infrared. *Appl. Opt.* **1997**, *36* (27), 7027–7036.

18. Mantsch, H. H.; Chapman, D. *Infrared Spectroscopy of Biomolecules*; Wiley-Liss, New York, 1996.

19. Tuminello, P. S.; Arakawa, E. T. Optical properties of Bacillus subtilis spores from 0.2 to 2.5um. *Appl. Opt.* **1997**, *36*, 13.

20. Helm, D.; Naumann, D. Identification of some bacterial cell components by FT-IR spectroscopy. *FEMS Microbiol. Lett.* **1995**, *126*, 75–80.

21. Wieliczka, D. M.; Querry, M. R. *Four Techniques to Measure Complex Refractive Indices of Liquids and Solids at Carbon Dioxide Laser Wavelengths in the Infrared Spectral Region*, U.S. Army Chemical Research, Development & Engineering Center; Technical Report, Report # CRDEC-CR-062, Jan. 1990.

Appendix A. Complex Indices of Refraction for DIMP, DMMP, DEP (*1*, *2*)

DIMP			DMMP			DEP		
λ (μm)	n	k	λ (μm)	n	k	λ (μm)	n	k
55.56	1.44	0.0000	55.56	1.50	0.0440	55.56	1.50	0.0000
52.63	1.45	0.0000	52.63	1.53	0.0450	52.63	1.51	0.0000
50.00	1.45	0.0000	50.00	1.51	0.0950	50.00	1.52	0.0000
47.62	1.46	0.0000	47.62	1.47	0.1020	47.62	1.52	0.0000
45.45	1.45	0.0000	45.45	1.46	0.0940	45.45	1.53	0.0000
43.48	1.46	0.0000	43.48	1.44	0.0750	43.48	1.53	0.0000
41.67	1.47	0.0000	41.67	1.43	0.0470	41.67	1.52	0.0000
40.00	1.48	0.0110	40.00	1.43	0.0330	40.00	1.53	0.0000
38.46	1.47	0.0240	38.46	1.45	0.0190	38.46	1.53	0.0000
37.04	1.46	0.0260	37.04	1.46	0.0140	37.04	1.53	0.0030
35.71	1.45	0.0240	35.71	1.48	0.0160	35.71	1.53	0.0050
34.48	1.44	0.0160	34.48	1.50	0.0280	34.48	1.53	0.0060
33.33	1.45	0.0080	33.33	1.50	0.0620	33.33	1.53	0.0120
32.26	1.45	0.0080	32.26	1.46	0.0860	32.26	1.53	0.0170
31.25	1.45	0.0060	31.25	1.42	0.0440	31.25	1.53	0.0230
30.30	1.45	0.0050	30.30	1.44	0.0170	30.30	1.53	0.0320
29.41	1.46	0.0010	29.41	1.46	0.0070	29.41	1.52	0.0400
28.57	1.47	0.0050	28.57	1.47	0.0040	28.57	1.51	0.0430
27.78	1.47	0.0050	27.78	1.48	0.0020	27.78	1.49	0.0350
27.03	1.48	0.0150	27.03	1.50	0.0060	27.03	1.50	0.0230
26.32	1.48	0.0240	26.32	1.52	0.0160	26.32	1.50	0.0160
25.64	1.47	0.0280	25.64	1.55	0.0490	25.64	1.51	0.0210
25.00	1.47	0.0310	25.00	1.53	0.1110	25.00	1.50	0.0280
24.39	1.47	0.0390	24.39	1.52	0.1260	24.39	1.49	0.0240
23.81	1.47	0.0450	23.81	1.39	0.1090	23.81	1.49	0.0110
23.26	1.45	0.0430	23.26	1.44	0.0350	23.26	1.49	0.0030
22.73	1.45	0.0330	22.73	1.47	0.0340	22.73	1.50	0.0030
22.22	1.46	0.0280	22.22	1.48	0.0530	22.22	1.50	0.0040
21.74	1.47	0.0260	21.74	1.80	0.0750	21.74	1.50	0.0020
21.28	1.48	0.0280	21.28	1.46	0.0990	21.28	1.51	0.0020
20.83	1.49	0.0440	20.83	1.46	0.0610	20.83	1.51	0.0000
20.41	1.50	0.0640	20.41	1.52	0.0740	20.41	1.51	0.0000
20.00	1.51	0.1470	20.00	1.46	0.2690	20.00	1.51	0.0000
19.61	1.39	0.1470	19.61	1.29	0.1050	19.61	1.51	0.0000
19.23	1.35	0.1000	19.23	1.35	0.0120	19.23	1.52	0.0030
18.87	1.36	0.0320	18.87	1.38	0.0070	18.87	1.52	0.0030
18.52	1.39	0.0180	18.52	1.41	0.0030	18.52	1.52	0.0030
18.18	1.40	0.0180	18.18	1.42	0.0020	18.18	1.52	0.0050
17.86	1.40	0.0140	17.86	1.43	0.0000	17.86	1.52	0.0240
17.54	1.41	0.0040	17.54	1.44	0.0000	17.54	1.50	0.0070
17.24	1.42	0.0040	17.24	1.45	0.0000	17.24	1.51	0.0000
16.95	1.42	0.0000	16.95	1.45	0.0000	16.95	1.52	0.0000
16.67	1.43	0.0000	16.67	1.46	0.0040	16.67	1.53	0.0000
16.39	1.44	0.0000	16.39	1.46	0.0040	16.39	1.53	0.0000
16.13	1.44	0.0000	16.13	1.48	0.0060	16.13	1.53	0.0010

15.87	1.44	0.0000	15.87	1.48	0.0060	15.87	1.53	0.0030
15.63	1.45	0.0020	15.63	1.48	0.0070	15.63	1.54	0.0030
15.38	1.45	0.0030	15.38	1.49	0.0050	15.38	1.54	0.0230
15.15	1.45	0.0000	15.15	1.49	0.0050	15.15	1.53	0.0020
14.93	1.46	0.0000	14.93	1.51	0.0090	14.93	1.54	0.0000
14.71	1.47	0.0020	14.71	1.51	0.0120	14.71	1.55	0.0010
14.49	1.47	0.0020	14.49	1.52	0.0140	14.49	1.57	0.0230
14.29	1.48	0.0090	14.29	1.54	0.0300	14.29	1.57	0.0420
14.08	1.50	0.0220	14.08	1.55	0.1050	14.08	1.53	0.0410
13.89	1.46	0.0600	13.89	1.46	0.0390	13.89	1.56	0.0170
13.70	1.45	0.0130	13.70	1.50	0.0120	13.70	1.60	0.0330
13.51	1.48	0.0150	13.51	1.52	0.0120	13.51	1.62	0.1550
13.33	1.48	0.0320	13.33	1.55	0.0150	13.33	1.44	0.1570
13.16	1.48	0.0140	13.16	1.58	0.0160	13.16	1.45	0.0590
12.99	1.50	0.0150	12.99	1.62	0.0370	12.99	1.47	0.0430
12.82	1.54	0.0340	12.82	1.71	0.1340	12.82	1.48	0.0450
12.66	1.50	0.1500	12.66	1.48	0.2940	12.66	1.47	0.0380
12.50	1.40	0.0680	12.50	1.48	0.0980	12.50	1.47	0.0200
12.35	1.43	0.0160	12.35	1.65	0.1610	12.35	1.48	0.0030
12.20	1.46	0.0090	12.20	1.40	0.4350	12.20	1.49	0.0030
12.05	1.47	0.0070	12.05	1.25	0.1220	12.05	1.51	0.0010
11.90	1.49	0.0040	11.90	1.37	0.0340	11.90	1.52	0.0070
11.76	1.50	0.0090	11.76	1.43	0.0210	11.76	1.52	0.0160
11.63	1.52	0.0090	11.63	1.47	0.0240	11.63	1.51	0.0310
11.49	1.54	0.0170	11.49	1.52	0.0240	11.49	1.49	0.0280
11.36	1.56	0.0290	11.36	1.56	0.0440	11.36	1.50	0.0050
11.24	1.59	0.0510	11.24	1.62	0.1300	11.24	1.51	0.0060
11.11	1.56	0.1190	11.11	1.57	0.2100	11.11	1.51	0.0010
10.99	1.57	0.1000	10.99	1.52	0.3170	10.99	1.52	0.0000
10.87	1.50	0.1240	10.87	1.30	0.2650	10.87	1.52	0.0000
10.75	1.54	0.0520	10.75	1.31	0.0820	10.75	1.53	0.0000
10.64	1.59	0.0500	10.64	1.39	0.0310	10.64	1.53	0.0000
10.53	1.66	0.0630	10.53	1.43	0.0220	10.53	1.54	0.0000
10.42	1.75	0.1040	10.42	1.48	0.0210	10.42	1.55	0.0050
10.31	1.93	0.2670	10.31	1.52	0.0230	10.31	1.55	0.0020
10.20	1.80	0.7420	10.20	1.56	0.0300	10.20	1.56	0.0020
10.10	1.33	0.7210	10.10	1.62	0.0420	10.10	1.58	0.0040
10.00	1.23	0.4890	10.00	1.70	0.0660	10.00	1.60	0.0190
9.90	1.20	0.5420	9.90	1.82	0.1440	9.90	1.60	0.0570
9.80	0.97	0.3800	9.80	1.95	0.4210	9.80	1.55	0.0700
9.71	1.02	0.1440	9.71	1.66	0.8130	9.71	1.57	0.0240
9.62	1.12	0.0640	9.62	1.25	0.6730	9.62	1.58	0.1030
9.52	1.19	0.0390	9.52	1.25	0.4930	9.52	1.57	0.0210
9.43	1.23	0.0250	9.43	1.14	0.5730	9.43	1.65	0.0360
9.35	1.27	0.0190	9.35	0.91	0.3570	9.35	1.66	0.2190
9.26	1.30	0.0190	9.26	1.01	0.1190	9.26	1.44	0.1290
9.17	1.34	0.0240	9.17	1.10	0.0610	9.17	1.54	0.0530
9.09	1.39	0.0570	9.09	1.17	0.0350	9.09	1.58	0.0620
9.01	1.33	0.1430	9.01	1.22	0.0310	9.01	1.63	0.1300
8.93	1.29	0.0610	8.93	1.25	0.0200	8.93	1.58	0.2280
8.85	1.32	0.0450	8.85	1.28	0.0190	8.85	1.48	0.2310
8.77	1.34	0.0830	8.77	1.30	0.0240	8.77	1.38	0.1850
8.70	1.31	0.0410	8.70	1.33	0.0180	8.70	1.39	0.0670

8.62	1.34	0.0360	8.62	1.36	0.0350	8.62	1.45	0.0400
8.55	1.36	0.0460	8.55	1.39	0.0500	8.55	1.48	0.0590
8.47	1.33	0.0740	8.47	1.38	0.0950	8.47	1.46	0.0340
8.40	1.34	0.0330	8.40	1.34	0.0950	8.40	1.49	0.0180
8.33	1.36	0.0280	8.33	1.35	0.0450	8.33	1.52	0.0150
8.26	1.39	0.0330	8.26	1.39	0.0400	8.26	1.54	0.0130
8.20	1.41	0.0350	8.20	1.46	0.0430	8.20	1.58	0.0180
8.13	1.47	0.0690	8.13	1.56	0.1040	8.13	1.61	0.0280
8.06	1.50	0.2450	8.06	1.59	0.3610	8.06	1.68	0.0740
8.00	1.23	0.2660	8.00	1.30	0.4440	8.00	1.70	0.1390
7.94	1.22	0.1170	7.94	1.12	0.3800	7.94	1.70	0.2350
7.87	1.23	0.0630	7.87	1.04	0.1300	7.87	1.70	0.3450
7.81	1.27	0.0340	7.81	1.15	0.0320	7.81	1.55	0.5030
7.75	1.30	0.0210	7.75	1.22	0.0250	7.75	1.30	0.5200
7.69	1.33	0.0220	7.69	1.28	0.0280	7.69	1.12	0.3270
7.63	1.33	0.0860	7.63	1.31	0.1310	7.63	1.15	0.1060
7.58	1.27	0.0320	7.58	1.19	0.0970	7.58	1.25	0.0420
7.52	1.31	0.0090	7.52	1.20	0.0190	7.52	1.31	0.0170
7.46	1.33	0.0150	7.46	1.24	0.0050	7.46	1.35	0.0150
7.41	1.34	0.0220	7.41	1.26	0.0000	7.41	1.36	0.0100
7.35	1.35	0.0210	7.35	1.28	0.0100	7.35	1.43	0.0340
7.30	1.38	0.0550	7.30	1.29	0.0010	7.30	1.34	0.0890
7.25	1.33	0.0700	7.25	1.30	0.0030	7.25	1.38	0.0230
7.19	1.27	0.0550	7.19	1.31	0.0080	7.19	1.39	0.0380
7.14	1.30	0.0130	7.14	1.31	0.0000	7.14	1.39	0.0200
7.09	1.32	0.0100	7.09	1.33	0.0080	7.09	1.40	0.0090
7.04	1.32	0.0150	7.04	1.32	0.0260	7.04	1.41	0.0080
6.99	1.32	0.0120	6.99	1.32	0.0170	6.99	1.43	0.0090
6.94	1.34	0.0120	6.94	1.33	0.0190	6.94	1.45	0.0270
6.90	1.34	0.0190	6.90	1.33	0.0280	6.90	1.42	0.0460
6.85	1.34	0.0230	6.85	1.32	0.0360	6.85	1.43	0.0270
6.80	1.32	0.0260	6.80	1.31	0.0330	6.80	1.42	0.0340
6.76	1.32	0.0040	6.76	1.31	0.0230	6.76	1.41	0.0260
6.71	1.33	0.0050	6.71	1.31	0.0130	6.71	1.41	0.0230
6.67	1.33	0.0050	6.67	1.31	0.0080	6.67	1.42	0.0010
6.62	1.33	0.0010	6.62	1.32	0.0050	6.62	1.43	0.0060
6.58	1.34	0.0020	6.58	1.32	0.0030	6.58	1.44	0.0020
6.54	1.34	0.0020	6.54	1.33	0.0020	6.54	1.44	0.0050
6.49	1.34	0.0020	6.49	1.33	0.0000	6.49	1.45	0.0040
6.45	1.34	0.0020	6.45	1.33	0.0010	6.45	1.45	0.0010
6.41	1.35	0.0000	6.41	1.34	0.0020	6.41	1.45	0.0050
6.37	1.35	0.0000	6.37	1.34	0.0030	6.37	1.47	0.0060
6.33	1.35	0.0000	6.33	1.34	0.0010	6.33	1.46	0.0260
6.29	1.35	0.0010	6.29	1.34	0.0000	6.29	1.47	0.0080
6.25	1.35	0.0010	6.25	1.34	0.0000	6.25	1.46	0.0280
6.21	1.35	0.0010	6.21	1.34	0.0010	6.21	1.46	0.0060
6.17	1.36	0.0010	6.17	1.34	0.0010	6.17	1.47	0.0040
6.13	1.36	0.0000	6.13	1.35	0.0010	6.14	1.48	0.0040
6.10	1.36	0.0010	6.10	1.35	0.0010	6.10	1.48	0.0030
6.06	1.36	0.0020	6.06	1.35	0.0010	6.06	1.49	0.0060
6.02	1.36	0.0030	6.02	1.35	0.0000	6.02	1.50	0.0050
5.99	1.36	0.0030	5.99	1.35	0.0000	5.99	1.52	0.0090
5.95	1.36	0.0020	5.95	1.35	0.0000	5.95	1.53	0.0150

5.92	1.36	0.0030	5.92	1.35	0.0000	5.92	1.56	0.0240
5.88	1.36	0.0040	5.88	1.36	0.0000	5.88	1.50	0.0350
5.85	1.36	0.0050	5.85	1.36	0.0000	5.85	1.64	0.1060
5.81	1.36	0.0040	5.81	1.36	0.0000	5.81	1.65	0.3460
5.78	1.36	0.0030	5.78	1.36	0.0010	5.78	1.39	0.4340
5.75	1.36	0.0010	5.75	1.36	0.0010	5.75	1.19	0.2600
5.71	1.36	0.0020	5.71	1.36	0.0020	5.71	1.22	0.0140
5.68	1.36	0.0040	5.68	1.36	0.0010	5.68	1.30	0.0280
5.65	1.36	0.0040	5.65	1.36	0.0000	5.65	1.34	0.0170
5.62	1.36	0.0010	5.62	1.36	0.0000	5.62	1.36	0.0090
5.59	1.36	0.0000	5.59	1.36	0.0000	5.59	1.37	0.0050
5.56	1.37	0.0000	5.56	1.36	0.0000	5.56	1.39	0.0020
5.52	1.37	0.0010	5.52	1.36	0.0010	5.52	1.39	0.0050
5.49	1.37	0.0010	5.49	1.36	0.0020	5.49	1.40	0.0040
5.46	1.37	0.0010	5.46	1.36	0.0020	5.46	1.41	0.0020
5.43	1.37	0.0000	5.43	1.37	0.0020	5.43	1.41	0.0030
5.41	1.37	0.0010	5.41	1.37	0.0030	5.41	1.41	0.0060
5.38	1.37	0.0010	5.38	1.36	0.0040	5.38	1.42	0.0030
5.35	1.37	0.0010	5.35	1.36	0.0030	5.35	1.42	0.0040
5.32	1.37	0.0010	5.32	1.36	0.0030	5.32	1.42	0.0030
5.29	1.37	0.0010	5.29	1.36	0.0010	5.29	1.43	0.0020
5.26	1.37	0.0020	5.26	1.36	0.0000	5.26	1.43	0.0030
5.24	1.37	0.0010	5.24	1.37	0.0000	5.24	1.43	0.0030
5.21	1.37	0.0010	5.21	1.37	0.0010	5.21	1.43	0.0020
5.18	1.37	0.0010	5.18	1.37	0.0020	5.18	1.43	0.0030
5.15	1.37	0.0020	5.15	1.38	0.0010	5.15	1.43	0.0030
5.13	1.37	0.0030	5.13	1.39	0.0010	5.13	1.44	0.0030
5.10	1.37	0.0030	5.10	1.37	0.0030	5.10	1.44	0.0030
5.08	1.37	0.0020	5.08	1.37	0.0040	5.08	1.44	0.0040
5.05	1.37	0.0030	5.05	1.37	0.0030	5.05	1.44	0.0060
5.03	1.37	0.0040	5.03	1.37	0.0030	5.03	1.44	0.0070
5.00	1.37	0.0050	5.00	1.37	0.0050	5.00	1.44	0.0060
4.98	1.37	0.0030	4.98	1.37	0.0060	4.98	1.44	0.0040
4.95	1.37	0.0020	4.95	1.37	0.0040	4.95	1.44	0.0030
4.93	1.37	0.0010	4.93	1.37	0.0020	4.93	1.44	0.0030
4.90	1.37	0.0010	4.90	1.37	0.0020	4.90	1.44	0.0030
4.88	1.37	0.0010	4.88	1.37	0.0020	4.88	1.44	0.0030
4.85	1.37	0.0030	4.85	1.37	0.0020	4.85	1.44	0.0020
4.83	1.37	0.0030	4.83	1.37	0.0010	4.83	1.44	0.0000
4.81	1.37	0.0030	4.81	1.37	0.0010	4.81	1.44	0.0000
4.78	1.37	0.0020	4.78	1.37	0.0000	4.78	1.44	0.0010
4.76	1.37	0.0030	4.76	1.37	0.0000	4.76	1.44	0.0020
4.74	1.37	0.0030	4.74	1.37	0.0000	4.74	1.44	0.0020
4.72	1.37	0.0020	4.72	1.37	0.0000	4.72	1.44	0.0020
4.69	1.37	0.0000	4.69	1.37	0.0000	4.69	1.45	0.0010
4.67	1.37	0.0000	4.67	1.37	0.0000	4.67	1.45	0.0010
4.65	1.37	0.0000	4.65	1.37	0.0000	4.65	1.45	0.0010
4.63	1.37	0.0000	4.63	1.37	0.0000	4.63	1.45	0.0000
4.61	1.37	0.0000	4.61	1.37	0.0010	4.61	1.45	0.0000
4.59	1.38	0.0000	4.59	1.37	0.0000	4.59	1.45	0.0000
4.57	1.38	0.0000	4.57	1.37	0.0000	4.57	1.45	0.0010
4.55	1.38	0.0000	4.55	1.37	0.0000	4.55	1.45	0.0000
4.52	1.38	0.0010	4.52	1.37	0.0000	4.52	1.45	0.0000

4.50	1.38	0.0020	4.50	1.37	0.0000	4.50	1.45	0.0000
4.48	1.38	0.0020	4.48	1.38	0.0000	4.48	1.45	0.0010
4.46	1.38	0.0000	4.46	1.38	0.0000	4.46	1.45	0.0010
4.44	1.38	0.0000	4.44	1.38	0.0000	4.44	1.45	0.0000
4.42	1.38	0.0010	4.42	1.38	0.0010	4.42	1.45	0.0000
4.41	1.38	0.0020	4.41	1.38	0.0000	4.41	1.45	0.0000
4.39	1.38	0.0000	4.39	1.38	0.0000	4.39	1.45	0.0010
4.37	1.38	0.0000	4.37	1.38	0.0000	4.37	1.45	0.0010
4.35	1.38	0.0010	4.35	1.38	0.0000	4.35	1.45	0.0000
4.33	1.38	0.0010	4.33	1.38	0.0000	4.33	1.45	0.0000
4.31	1.38	0.0000	4.31	1.38	0.0000	4.31	1.45	0.0010
4.29	1.38	0.0000	4.29	1.38	0.0000	4.29	1.45	0.0010
4.27	1.38	0.0000	4.27	1.38	0.0000	4.27	1.45	0.0020
4.26	1.38	0.0000	4.26	1.38	0.0000	4.26	1.45	0.0010
4.24	1.38	0.0000	4.24	1.38	0.0000	4.24	1.45	0.0020
4.22	1.38	0.0000	4.22	1.38	0.0000	4.22	1.45	0.0000
4.20	1.38	0.0000	4.20	1.38	0.0000	4.20	1.45	0.0000
4.18	1.38	0.0000	4.18	1.38	0.0000	4.18	1.45	0.0000
4.17	1.38	0.0010	4.17	1.38	0.0000	4.17	1.46	0.0000
4.15	1.38	0.0000	4.15	1.38	0.0000	4.15	1.46	0.0000
4.13	1.38	0.0000	4.13	1.38	0.0010	4.13	1.46	0.0000
4.12	1.38	0.0000	4.12	1.38	0.0010	4.12	1.45	0.0000
4.10	1.38	0.0000	4.10	1.38	0.0000	4.10	1.46	0.0000
4.08	1.38	0.0000	4.08	1.38	0.0000	4.08	1.46	0.0000
4.07	1.38	0.0000	4.07	1.38	0.0000	4.07	1.46	0.0000
4.05	1.38	0.0000	4.05	1.38	0.0000	4.05	1.46	0.0000
4.03	1.38	0.0000	4.03	1.38	0.0000	4.03	1.46	0.0000
4.02	1.38	0.0000	4.02	1.38	0.0000	4.02	1.46	0.0000
4.00	1.38	0.0000	4.00	1.38	0.0000	4.00	1.46	0.0000
3.98	1.38	0.0000	3.98	1.38	0.0000	3.98	1.46	0.0000
3.97	1.38	0.0000	3.97	1.38	0.0000	3.97	1.46	0.0000
3.95	1.38	0.0000	3.95	1.38	0.0000	3.95	1.46	0.0000
3.94	1.38	0.0000	3.94	1.38	0.0000	3.94	1.46	0.0000
3.92	1.38	0.0000	3.92	1.38	0.0000	3.92	1.46	0.0000
3.91	1.38	0.0000	3.91	1.39	0.0000	3.91	1.47	0.0030
3.89	1.38	0.0000	3.89	1.39	0.0000	3.89	1.46	0.0000
3.88	1.38	0.0010	3.88	1.38	0.0000	3.88	1.46	0.0000
3.86	1.38	0.0000	3.86	1.39	0.0000	3.86	1.46	0.0000
3.85	1.38	0.0000	3.85	1.39	0.0010	3.85	1.46	0.0000
3.83	1.38	0.0010	3.83	1.38	0.0030	3.83	1.46	0.0000
3.82	1.38	0.0030	3.82	1.38	0.0010	3.82	1.46	0.0000
3.80	1.38	0.0010	3.80	1.38	0.0000	3.80	1.46	0.0010
3.79	1.39	0.0000	3.79	1.39	0.0000	3.79	1.46	0.0010
3.77	1.39	0.0000	3.77	1.39	0.0000	3.77	1.46	0.0000
3.76	1.39	0.0000	3.76	1.39	0.0010	3.76	1.46	0.0000
3.75	1.39	0.0010	3.75	1.39	0.0010	3.75	1.46	0.0000
3.73	1.39	0.0010	3.73	1.38	0.0010	3.73	1.46	0.0000
3.72	1.39	0.0000	3.72	1.38	0.0000	3.72	1.46	0.0000
3.70	1.39	0.0010	3.70	1.39	0.0000	3.70	1.46	0.0000
3.69	1.39	0.0010	3.69	1.39	0.0000	3.69	1.46	0.0000
3.68	1.39	0.0010	3.68	1.39	0.0000	3.68	1.46	0.0000
3.66	1.39	0.0000	3.66	1.39	0.0000	3.66	1.47	0.0000
3.65	1.39	0.0000	3.65	1.39	0.0020	3.65	1.46	0.0000

3.64	1.39	0.0000	3.64	1.39	0.0030	3.64	1.46	0.0000
3.62	1.39	0.0000	3.62	1.39	0.0040	3.62	1.46	0.0000
3.61	1.39	0.0010	3.61	1.39	0.0020	3.61	1.46	0.0010
3.60	1.39	0.0020	3.60	1.39	0.0000	3.60	1.46	0.0010
3.58	1.39	0.0030	3.58	1.39	0.0000	3.58	1.46	0.0000
3.57	1.39	0.0010	3.57	1.39	0.0020	3.57	1.46	0.0000
3.56	1.39	0.0000	3.56	1.39	0.0020	3.56	1.47	0.0000
3.55	1.39	0.0010	3.55	1.39	0.0010	3.55	1.47	0.0000
3.53	1.39	0.0020	3.53	1.40	0.0030	3.53	1.47	0.0010
3.52	1.39	0.0030	3.52	1.40	0.0110	3.52	1.47	0.0000
3.51	1.39	0.0030	3.51	1.39	0.0160	3.51	1.47	0.0000
3.50	1.40	0.0050	3.50	1.39	0.0140	3.50	1.47	0.0030
3.48	1.40	0.0060	3.48	1.38	0.0080	3.48	1.47	0.0050
3.47	1.39	0.0140	3.47	1.39	0.0050	3.47	1.47	0.0030
3.46	1.39	0.0060	3.46	1.39	0.0060	3.46	1.47	0.0050
3.45	1.40	0.0050	3.45	1.39	0.0080	3.45	1.48	0.0100
3.44	1.40	0.0110	3.44	1.39	0.0120	3.44	1.46	0.0030
3.42	1.40	0.0170	3.42	1.39	0.0130	3.42	1.47	0.0070
3.41	1.40	0.0270	3.41	1.40	0.0150	3.41	1.47	0.0120
3.40	1.38	0.0240	3.40	1.39	0.0230	3.40	1.47	0.0090
3.39	1.39	0.0170	3.39	1.39	0.0290	3.39	1.47	0.0100
3.38	1.40	0.0190	3.38	1.38	0.0260	3.38	1.47	0.0130
3.37	1.41	0.0430	3.37	1.37	0.0180	3.37	1.47	0.0180
3.36	1.36	0.0670	3.36	1.38	0.0150	3.36	1.46	0.0300
3.34	1.34	0.0310	3.34	1.38	0.0180	3.34	1.45	0.0240
3.33	1.35	0.0070	3.33	1.37	0.0180	3.33	1.45	0.0150
3.32	1.35	0.0010	3.32	1.37	0.0130	3.32	1.45	0.0060
3.31	1.36	0.0000	3.31	1.37	0.0070	3.31	1.45	0.0020
3.30	1.37	0.0000	3.30	1.37	0.0040	3.30	1.45	0.0010
3.29	1.37	0.0000	3.29	1.37	0.0020	3.29	1.45	0.0000
3.28	1.37	0.0000	3.28	1.37	0.0010	3.28	1.46	0.0010
3.27	1.37	0.0000	3.27	1.38	0.0000	3.27	1.46	0.0020
3.26	1.37	0.0000	3.26	1.38	0.0000	3.26	1.46	0.0020
3.25	1.37	0.0000	3.25	1.38	0.0000	3.25	1.46	0.0030
3.24	1.37	0.0000	3.24	1.38	0.0000	3.24	1.46	0.0010
3.23	1.37	0.0000	3.23	1.38	0.0010	3.23	1.46	0.0000
3.22	1.38	0.0000	3.22	1.38	0.0010	3.22	1.46	0.0000
3.21	1.38	0.0000	3.21	1.38	0.0010	3.21	1.46	0.0000
3.19	1.38	0.0000	3.19	1.38	0.0000	3.19	1.46	0.0000
3.18	1.38	0.0000	3.18	1.38	0.0000	3.18	1.46	0.0000
3.17	1.38	0.0000	3.17	1.38	0.0000	3.17	1.46	0.0000
3.16	1.38	0.0000	3.16	1.38	0.0000	3.16	1.46	0.0000
3.15	1.38	0.0000	3.15	1.38	0.0010	3.15	1.46	0.0000
3.14	1.38	0.0000	3.14	1.38	0.0000	3.14	1.46	0.0000
3.13	1.38	0.0000	3.13	1.38	0.0000	3.13	1.46	0.0000
3.13	1.38	0.0010	3.13	1.38	0.0000	3.13	1.46	0.0000
3.12	1.38	0.0000	3.12	1.38	0.0000	3.12	1.46	0.0010
3.11	1.38	0.0000	3.11	1.38	0.0000	3.11	1.46	0.0000
3.10	1.38	0.0000	3.10	1.36	0.0000	3.10	1.46	0.0000
3.09	1.38	0.0000	3.09	1.38	0.0000	3.09	1.46	0.0000
3.08	1.38	0.0000	3.08	1.38	0.0000	3.08	1.46	0.0000
3.07	1.38	0.0000	3.07	1.38	0.0000	3.07	1.45	0.0000
3.06	1.38	0.0000	3.06	1.38	0.0000	3.06	1.48	0.0000

3.05	1.38	0.0000	3.05	1.38	0.0000	3.05	1.46	0.0000
3.04	1.38	0.0000	3.04	1.39	0.0010	3.04	1.46	0.0000
3.03	1.38	0.0000	3.03	1.38	0.0010	3.03	1.46	0.0000
3.02	1.38	0.0000	3.02	1.38	0.0000	3.02	1.46	0.0000
3.01	1.39	0.0000	3.01	1.38	0.0000	3.01	1.45	0.0000
3.00	1.39	0.0000	3.00	1.39	0.0000	3.00	1.46	0.0000
2.99	1.38	0.0000	2.99	1.39	0.0000	2.99	1.47	0.0000
2.99	1.38	0.0000	2.99	1.39	0.0000	2.99	1.46	0.0000
2.98	1.38	0.0000	2.98	1.38	0.0000	2.98	1.47	0.0000
2.97	1.38	0.0000	2.97	1.38	0.0000	2.97	1.46	0.0000
2.96	1.38	0.0000	2.96	1.38	0.0000	2.96	1.47	0.0000
2.95	1.38	0.0000	2.95	1.39	0.0000	2.95	1.49	0.0000
2.94	1.39	0.0000	2.94	1.39	0.0000	2.94	1.47	0.0000
2.93	1.39	0.0000	2.93	1.39	0.0000	2.93	1.47	0.0000
2.92	1.39	0.0000	2.92	1.39	0.0010	2.92	1.47	0.0000
2.92	1.38	0.0010	2.92	1.38	0.0000	2.92	1.46	0.0000
2.91	1.38	0.0000	2.91	1.38	0.0000	2.91	1.47	0.0000
2.90	1.38	0.0000	2.90	1.39	0.0000	2.90	1.47	0.0000
2.89	1.38	0.0000	2.89	1.39	0.0000	2.89	1.47	0.0000
2.88	1.38	0.0000	2.88	1.39	0.0000	2.88	1.47	0.0000
2.87	1.38	0.0000	2.87	1.39	0.0000	2.87	1.47	0.0000
2.87	1.39	0.0000	2.87	1.39	0.0000	2.87	1.47	0.0000
2.86	1.39	0.0000	2.86	1.39	0.0000	2.86	1.47	0.0000
2.85	1.39	0.0000	2.85	1.39	0.0000	2.85	1.47	0.0000
2.84	1.39	0.0000	2.84	1.39	0.0000	2.84	1.47	0.0000
2.83	1.39	0.0000	2.83	1.39	0.0000	2.83	1.46	0.0000
2.82	1.38	0.0000	2.82	1.39	0.0000	2.82	1.47	0.0000
2.82	1.38	0.0000	2.82	1.39	0.0000	2.82	1.47	0.0000
2.81	1.39	0.0000	2.81	1.39	0.0000	2.81	1.47	0.0000
2.80	1.39	0.0000	2.80	1.39	0.0000	2.80	1.47	0.0000
2.79	1.39	0.0000	2.79	1.39	0.0000	2.79	1.47	0.0000
2.79	1.38	0.0000	2.79	1.39	0.0000	2.79	1.47	0.0000
2.78	1.39	0.0000	2.78	1.39	0.0000	2.78	1.47	0.0000
2.77	1.38	0.0000	2.77	1.39	0.0000	2.77	1.47	0.0000
2.76	1.39	0.0000	2.76	1.39	0.0000	2.76	1.47	0.0000
2.75	1.39	0.0000	2.75	1.39	0.0000	2.75	1.46	0.0010
2.75	1.39	0.0000	2.75	1.39	0.0000	2.75	1.47	0.0000
2.74	1.38	0.0000	2.74	1.39	0.0010	2.74	1.47	0.0000
2.73	1.39	0.0000	2.73	1.39	0.0000	2.73	1.47	0.0000
2.72	1.39	0.0000	2.72	1.39	0.0000	2.72	1.47	0.0000
2.72	1.39	0.0000	2.72	1.39	0.0000	2.72	1.47	0.0000
2.71	1.39	0.0000	2.71	1.39	0.0000	2.71	1.47	0.0000
2.70	1.39	0.0000	2.70	1.39	0.0000	2.70	1.47	0.0000
2.70	1.39	0.0000	2.70	1.39	0.0000	2.70	1.47	0.0000
2.69	1.39	0.0000	2.69	1.39	0.0000	2.69	1.47	0.0000
2.68	1.39	0.0000	2.68	1.39	0.0000	2.68	1.47	0.0000
2.67	1.39	0.0000	2.67	1.39	0.0000	2.67	1.47	0.0000
2.67	1.39	0.0000	2.67	1.39	0.0000	2.67	1.47	0.0000
2.66	1.39	0.0000	2.66	1.39	0.0000	2.66	1.47	0.0000
2.65	1.39	0.0000	2.65	1.39	0.0000	2.65	1.47	0.0000
2.65	1.39	0.0000	2.65	1.39	0.0000	2.65	1.47	0.0000
2.64	1.39	0.0000	2.64	1.39	0.0010	2.64	1.47	0.0000
2.63	1.39	0.0000	2.63	1.39	0.0010	2.63	1.47	0.0000

2.62	1.39	0.0000	2.62	1.39	0.0020	2.62	1.47	0.0000
2.62	1.39	0.0000	2.62	1.39	0.0020	2.62	1.46	0.0000
2.61	1.39	0.0000	2.61	1.39	0.0010	2.61	1.47	0.0000
2.60	1.39	0.0000	2.60	1.39	0.0000	2.60	1.47	0.0000
2.60	1.39	0.0000	2.60	1.39	0.0000	2.60	1.47	0.0000
2.59	1.39	0.0000	2.59	1.39	0.0010	2.59	1.47	0.0000
2.58	1.39	0.0000	2.58	1.39	0.0010	2.58	1.47	0.0000
2.58	1.39	0.0000	2.58	1.39	0.0000	2.58	1.47	0.0000
2.57	1.39	0.0000	2.57	1.39	0.0000	2.57	1.47	0.0000
2.56	1.39	0.0000	2.56	1.39	0.0000	2.56	1.47	0.0000
2.56	1.39	0.0000	2.56	1.39	0.0000	2.56	1.47	0.0000
2.55	1.39	0.0000	2.55	1.39	0.0000	2.55	1.47	0.0000
2.54	1.39	0.0000	2.54	1.39	0.0000	2.54	1.47	0.0000
2.54	1.39	0.0000	2.54	1.39	0.0000	2.54	1.47	0.0000
2.53	1.39	0.0000	2.53	1.39	0.0000	2.53	1.47	0.0000
2.53	1.39	0.0000	2.53	1.39	0.0000	2.53	1.47	0.0000
2.52	1.39	0.0000	2.52	1.39	0.0000	2.52	1.47	0.0000
2.51	1.39	0.0000	2.51	1.39	0.0010	2.51	1.47	0.0000
2.51	1.39	0.0000	2.51	1.39	0.0000	2.51	1.47	0.0000
2.50	1.39	0.0000	2.50	1.39	0.0000	2.50	1.47	0.0000
2.50	1.41	0.0003	2.50	1.40	0.0005	2.50	1.49	0.0003
2.48	1.41	0.0004	2.49	1.40	0.0006	2.49	1.49	0.0003
2.46	1.41	0.0005	2.48	1.40	0.0006	2.48	1.49	0.0004
2.44	1.41	0.0006	2.47	1.40	0.0007	2.47	1.49	0.0004
2.42	1.41	0.0005	2.46	1.40	0.0007	2.46	1.49	0.0003
2.40	1.41	0.0004	2.45	1.40	0.0005	2.45	1.49	0.0006
2.38	1.41	0.0003	2.44	1.40	0.0004	2.44	1.49	0.0006
2.36	1.41	0.0003	2.43	1.40	0.0004	2.43	1.49	0.0006
2.34	1.41	0.0005	2.42	1.40	0.0004	2.42	1.49	0.0006
2.32	1.41	0.0009	2.41	1.40	0.0004	2.41	1.49	0.0006
2.30	1.41	0.0008	2.40	1.40	0.0005	2.40	1.49	0.0005
2.28	1.41	0.0006	2.39	1.40	0.0006	2.39	1.49	0.0004
2.26	1.41	0.0006	2.38	1.40	0.0006	2.38	1.49	0.0004
2.24	1.41	0.0002	2.37	1.40	0.0004	2.37	1.49	0.0003
2.22	1.41	0.0001	2.36	1.40	0.0003	2.36	1.49	0.0004
2.20	1.41	0.0001	2.35	1.40	0.0004	2.35	1.49	0.0005
2.18	1.41	0.0001	2.34	1.40	0.0003	2.34	1.49	0.0005
2.16	1.41	0.0001	2.33	1.41	0.0004	2.33	1.49	0.0004
2.14	1.41	0.0001	2.32	1.41	0.0005	2.32	1.49	0.0004
2.12	1.41	0.0001	2.31	1.41	0.0003	2.31	1.49	0.0006
2.10	1.41	0.0001	2.30	1.41	0.0003	2.30	1.49	0.0007
2.08	1.41	0.0000	2.29	1.41	0.0004	2.29	1.49	0.0005
2.06	1.41	0.0000	2.28	1.41	0.0006	2.28	1.49	0.0004
2.04	1.41	0.0000	2.27	1.41	0.0013	2.27	1.49	0.0005
2.02	1.41	0.0000	2.26	1.41	0.0012	2.26	1.49	0.0008
2.00	1.41	0.0000	2.25	1.41	0.0012	2.25	1.49	0.0005
1.98	1.41	0.0000	2.24	1.40	0.0009	2.24	1.49	0.0003
1.96	1.41	0.0000	2.23	1.40	0.0006	2.23	1.49	0.0002
1.94	1.41	0.0000	2.22	1.40	0.0004	2.22	1.49	0.0001
1.92	1.41	0.0000	2.21	1.41	0.0002	2.21	1.49	0.0001
1.90	1.41	0.0000	2.20	1.41	0.0002	2.20	1.49	0.0001
1.88	1.41	0.0000	2.19	1.41	0.0001	2.19	1.49	0.0001
1.86	1.41	0.0000	2.18	1.41	0.0001	2.18	1.49	0.0001

1.84	1.41	0.0000	2.17	1.41	0.0001	2.17	1.49	0.0001
1.82	1.41	0.0000	2.16	1.41	0.0001	2.16	1.49	0.0002
1.80	1.41	0.0000	2.15	1.41	0.0001	2.15	1.49	0.0001
1.78	1.41	0.0000	2.14	1.41	0.0000	2.14	1.49	0.0002
1.76	1.41	0.0001	2.13	1.41	0.0000	2.13	1.49	0.0001
1.74	1.41	0.0001	2.12	1.41	0.0000	2.12	1.49	0.0001
1.72	1.41	0.0001	2.11	1.41	0.0000	2.11	1.49	0.0001
1.70	1.41	0.0001	2.10	1.41	0.0000	2.10	1.49	0.0000
1.68	1.41	0.0001	2.09	1.41	0.0000	2.09	1.49	0.0000
1.66	1.41	0.0000	2.08	1.41	0.0000	2.08	1.49	0.0000
1.64	1.41	0.0000	2.07	1.41	0.0000	2.07	1.49	0.0000
1.62	1.41	0.0000	2.06	1.41	0.0000	2.06	1.49	0.0000
1.59	1.41	0.0000	2.05	1.41	0.0000	2.05	1.49	0.0000
1.57	1.41	0.0000	2.04	1.41	0.0000	2.04	1.49	0.0000
1.55	1.41	0.0000	2.03	1.41	0.0000	2.03	1.49	0.0000
1.53	1.41	0.0000	2.02	1.41	0.0000	2.02	1.49	0.0000
1.51	1.41	0.0000	2.01	1.41	0.0000	2.01	1.49	0.0000
1.49	1.41	0.0000	2.00	1.41	0.0000	2.00	1.49	0.0000
1.47	1.41	0.0000	1.99	1.41	0.0000	1.99	1.49	0.0000
1.45	1.41	0.0000	1.98	1.41	0.0000	1.98	1.49	0.0000
1.43	1.41	0.0000	1.97	1.41	0.0000	1.97	1.49	0.0000
1.41	1.41	0.0000	1.96	1.41	0.0000	1.96	1.49	0.0000
1.39	1.41	0.0000	1.95	1.41	0.0000	1.95	1.49	0.0000
1.37	1.41	0.0000	1.94	1.41	0.0000	1.94	1.49	0.0000
1.35	1.41	0.0000	1.93	1.41	0.0000	1.93	1.50	0.0000
1.33	1.41	0.0000	1.92	1.41	0.0000	1.92	1.50	0.0000
1.31	1.41	0.0000	1.91	1.41	0.0000	1.91	1.50	0.0000
1.29	1.41	0.0000	1.90	1.41	0.0000	1.90	1.50	0.0000
1.27	1.41	0.0000	1.89	1.41	0.0000	1.89	1.50	0.0000
1.25	1.41	0.0000	1.88	1.41	0.0000	1.88	1.50	0.0000
1.23	1.41	0.0000	1.87	1.41	0.0000	1.87	1.50	0.0000
1.21	1.41	0.0000	1.86	1.41	0.0000	1.86	1.50	0.0000
1.19	1.41	0.0000	1.85	1.41	0.0000	1.85	1.50	0.0000
1.17	1.41	0.0000	1.84	1.41	0.0000	1.84	1.50	0.0000
1.15	1.41	0.0000	1.83	1.41	0.0000	1.83	1.50	0.0000
1.13	1.41	0.0000	1.82	1.41	0.0000	1.82	1.50	0.0000
1.11	1.41	0.0000	1.81	1.41	0.0000	1.81	1.50	0.0000
1.09	1.41	0.0000	1.80	1.41	0.0000	1.80	1.50	0.0000
1.07	1.41	0.0000	1.79	1.41	0.0000	1.79	1.50	0.0000
1.05	1.41	0.0000	1.78	1.41	0.0000	1.78	1.50	0.0000
1.03	1.41	0.0000	1.77	1.41	0.0000	1.77	1.50	0.0000
1.01	1.41	0.0000	1.76	1.41	0.0000	1.76	1.50	0.0000
0.99	1.41	0.0000	1.75	1.41	0.0000	1.75	1.50	0.0000
0.97	1.41	0.0000	1.74	1.41	0.0000	1.74	1.50	0.0000
0.95	1.41	0.0000	1.73	1.41	0.0001	1.73	1.50	0.0001
0.93	1.42	0.0000	1.72	1.41	0.0001	1.72	1.50	0.0001
0.91	1.42	0.0000	1.71	1.41	0.0001	1.71	1.50	0.0001
0.89	1.42	0.0000	1.70	1.41	0.0001	1.70	1.50	0.0001
0.87	1.42	0.0000	1.69	1.41	0.0001	1.69	1.50	0.0001
0.85	1.42	0.0000	1.68	1.41	0.0001	1.68	1.50	0.0001
0.83	1.42	0.0000	1.67	1.41	0.0001	1.67	1.50	0.0001
0.81	1.42	0.0000	1.66	1.41	0.0001	1.66	1.50	0.0001

1. Querry, Marvin R. *Optical constants of minerals and other materials from the millimeter to the ultraviolet*; Chemical Research, Development and Engineering Center technical report, CRDEC-CR88009; November 1987.

2. Wieliczka, D. M.; Querry, M. R. *Four Techniques to Measure Complex Refractive Indices of Liquids and Solids at Carbon Dioxide Laser Wavelengths in the Infrared Spectral Region*; U.S. Army Chemical Research, Development & Engineering Center Technical Report, Report # CRDEC-CR-062, January 1990.

Appendix B. IR Absorptance Spectra for DMMP, DIMP, and DEMP

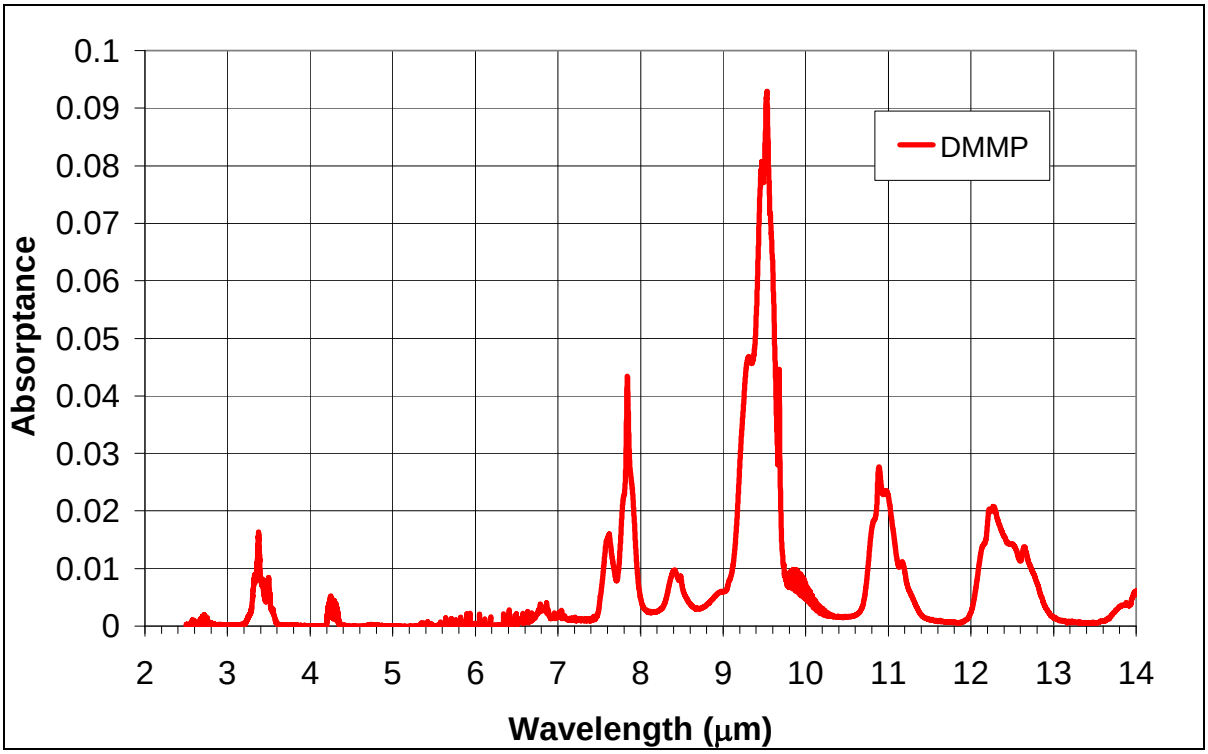

Figure B-1. Measured absorptance spectra for 1 cm path of liquid phase dimethyl-methylphosphonate (DMMP).

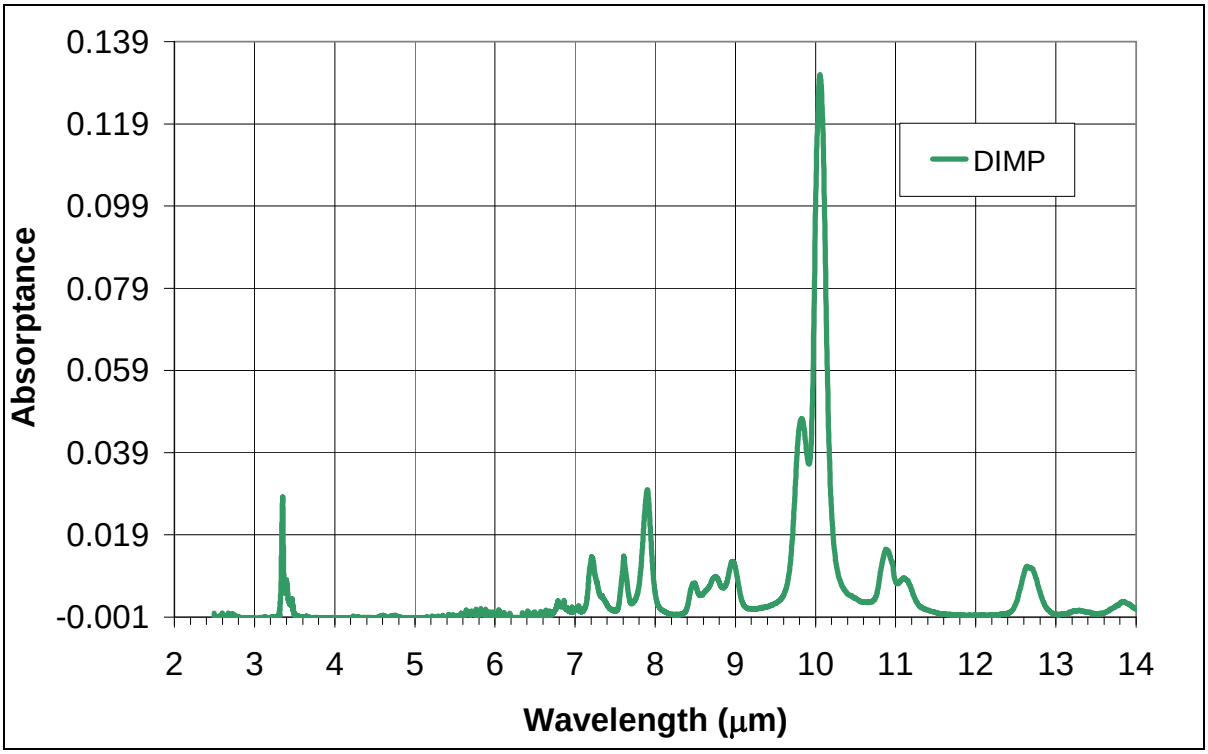

Figure B-2. Measured absorptance spectra for 1 cm path of liquid phase diisopropyl-methylphosphonate (DIMP).

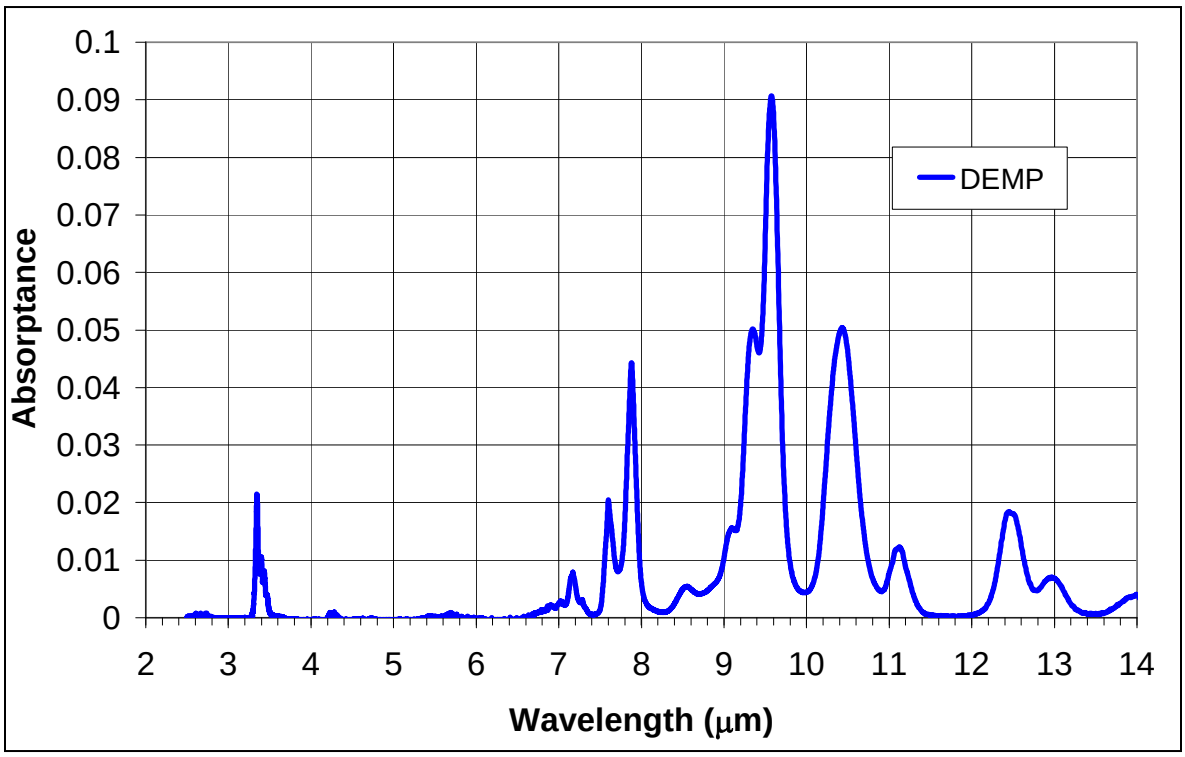

Figure B-3. Measured absorptance spectra for 1 cm path of liquid diethyl methylphosphonate (DEMP).

INTENTIONALLY LEFT BLANK

Distribution List

ADMNSTR
DEFNS TECHL INFO CTR
ATTN DTIC-OCP (ELECTRONIC COPY)
8725 JOHN J KINGMAN RD STE 0944
FT BELVOIR VA 22060-6218

EDGEWOOD CHEMICAL BIOLOGICAL CTR
ATTN AMSRD-ECB-RT-DP
A C SAMUELS
ATTN AMSSB-RRT-DP
R VANDERBEEK
5183 BLACKHAWK RD BLDG E-5554
ABERDEEN PROVING GROUND MD 21010-5424

ERDEC RESEARCH & TECHNOLOGY DIRECTORATE
ATTN SCBRD-RTB D ANDERSON
5183 BLACKHAWK RD BLDG E3724
ABERDEEN PROVING GROUND MD 21010-5423

US ARMY ECBC
ATTN AMSRD-ECB-RT-TA BOTTIGER
5183 BLACKHAWK RD BLDG E-5951
ABERDEEN PROVING GROUND MD 21010-5424

US ARMY RSRCH LAB
ATTN AMSRD-ARL-CI-OK-TP TECHL LIB T LANDFRIED
BLDG 4600
ABERDEEN PROVING GROUND MD 21005-5066

US ARMY TESTS & EVALUATION COMMAND
ATTN AMSTE-TM-S C CHAN
732 LONG CORNER RD
ABERDEEN PROVING GROUND MD 21005-5055

USAF ARMSTRONG LAB EDGEWOOD RDEC
ATTN SCBRD-RTB R DOHERTY
5101 HOADLEY RD
ABERDEEN PROVING GROUND MD 21010-5423

US GOVERNMENT PRINT OFF
DEPOSITORY RECEIVING SECTION
ATTN MAIL STOP IDAD J TATE
732 NORTH CAPITOL ST., NW
WASHINGTON DC 20402

DIRECTOR
US ARMY RSRCH LAB
ATTN AMSRD-ARL-RO-EV W D BACH
PO BOX 12211
RESEARCH TRIANGLE PARK NC 27709

US ARMY RSRCH LAB
ATTN AMSRD-ARL-CI-ES K GURTON (10 COPIES)
ATTN AMSRD-ARL-CI-OK-T TECHL PUB (2 COPIES)
ATTN AMSRD-ARL-CI-OK-TL TECHL LIB (2 COPIES)
ATTN AMSRD-ARL-D J M MILLER
ATTN IMNE-ALC-IMS MAIL & RECORDS MGMT
ADELPHI, MD 20783-1197

INTENTIONALLY LEFT BLANK